Testing and Analysis of a Composite Non-Cylindrical Aircraft Fuselage Structure, Part II: Severe Damage

Adam Przekop,[1] Dawn C. Jegley,[1] Andrew E. Lovejoy,[1] Marshall Rouse[2]
NASA Langley Research Center, Hampton, VA 23681

and

Hsi-Yung T. Wu[3]
The Boeing Company, Huntington Beach, CA 92647

The Environmentally Responsible Aviation Project aimed to develop aircraft technologies enabling significant fuel burn and community noise reductions. Small incremental changes to the conventional metallic alloy-based 'tube and wing' configuration were not sufficient to achieve the desired metrics. One airframe concept identified by the project as having the potential to dramatically improve aircraft performance was a composite-based hybrid wing body configuration. Such a concept, however, presented inherent challenges stemming from, among other factors, the necessity to transfer wing loads through the entire center fuselage section which accommodates a pressurized cabin confined by flat or nearly flat panels. This paper discusses a finite element analysis and the testing of a large-scale hybrid wing body center section structure developed and constructed to demonstrate that the Pultruded Rod Stitched Efficient Unitized Structure concept can meet these challenging demands of the next generation airframes. Part II of the paper considers the final test to failure of the test article in the presence of an intentionally inflicted severe discrete source damage under the wing up-bending loading condition. Finite element analysis results are compared with measurements acquired during the test and demonstrate that the hybrid wing body test article was able to redistribute and support the required design loads in a severely damaged condition.

I. Introduction

The primary structural concept pursued as an important component of next generation airframe technology under the Environmentally Responsible Aviation (ERA) Project at NASA was the Pultruded Rod Stitched Efficient Unitized Structure (PRSEUS),[1-18] illustrated in Fig. 1. This concept, developed in a collaboration between NASA and The Boeing Company, is intended for application to future transport aircraft with the goal of developing lighter structure so that the aircraft will require less fuel and produce fewer pollutants. The PRSEUS structure is highly integrated, structurally efficient, and has damage-arresting capabilities. In this concept, a stitched carbon-epoxy material system is used. By stitching through the thickness of a dry material system, the labor associated with panel fabrication and assembly can be significantly reduced. When stitching through the thickness of pre-stacked skin, stringers, and frames, the need for mechanical fasteners is almost eliminated. In addition, stitching reduces

[1] Senior Aerospace Research Engineer, Structural Mechanics and Concepts Branch, Mail Stop 190, 8 West Taylor Street, Associate Fellow AIAA.
[2] Senior Aerospace Research Engineer, Structural Testing Branch, Mail Stop 190, 8 West Taylor Street, Senior Member AIAA.
[3] Associate Technical Fellow, Boeing Research and Technology, MC H017-D601, 14900 Bolsa Road.

delamination and improves damage tolerance, allowing for a lighter structure with more gradual failures than traditional composites which do not have through-the-thickness reinforcement.

The PRSEUS concept consists of carbon-epoxy panels fabricated from dry components stitched together, after which the resin is infused in an oven while the panel is subjected to vacuum pressure. Skins, flanges, and webs are composed of layers of carbon material that are knitted into multi-ply stacks. A single stack has the thickness of 0.052 in. and comprises seven plies with stacking sequence [+45, −45, 0, 90, 0, −45, +45] and percentage of the 0, 45 and 90-degree fibers equal to 44.9, 42.9, and 12.2, respectively. Several knitted stacks are used to build up the desired thickness and configuration. Stiffener flanges are stitched to the skin using Vectran® thread and no mechanical fasteners are used for joining. To maintain the panel geometry during fabrication, first stiffeners and then the skin are placed in a tool for stitching prior to moving the assembly to a curing tool for consolidation in the oven. The stiffeners running in the S direction in Fig. 1a (stringers) consist of webs with unidirectional carbon fiber rods at the top of the web. The stack material forming the stiffener web overwraps the rod to form the stiffener cap. The stiffeners in the F direction in Fig. 1a (frames) are foam-filled sandwich structures. The manufacturing process is described in detail in Ref. 6.

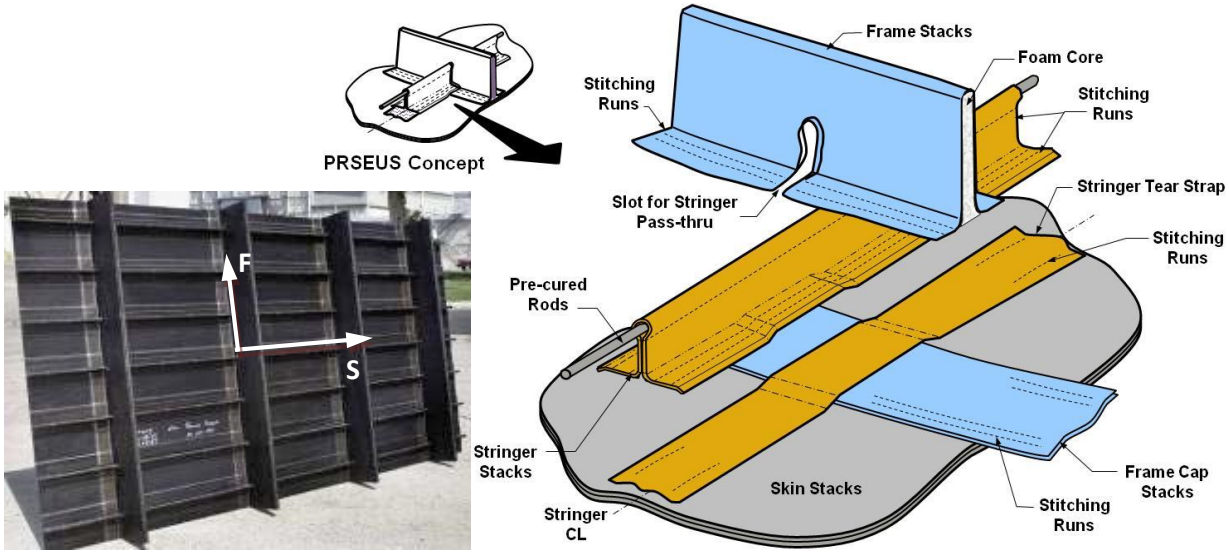

(a) **(b)**

Figure 1. PRSEUS: (a) sample flat panel and (b) general assembly concept.

Numerous test articles utilizing the PRSEUS concept have been built and tested. Typically only individual load conditions such as tension,[9,13] compression[7,9,12] or pressure[8,9,11] were applied as a conventional building-block approach was followed. However, testing under the combined load environment, inherent to the center section of a hybrid wing body (HWB) airframe, had not been conducted prior to the tests described in part I of this paper.[18] As illustrated in Fig. 2, the top center section of a HWB fuselage is required to sustain loads in each of the three primary directions,[15,16] namely stream-wise (Nx), span-wise (Ny), and normal (Nz). Given the specific PRSEUS panel orientation shown in Fig. 2, the wing bending loads, Ny, are carried primarily by the frame members. Consequently, severe damage to a crown panel frame can adversely affect structural integrity of the HWB airframe under increased maneuvering loads.

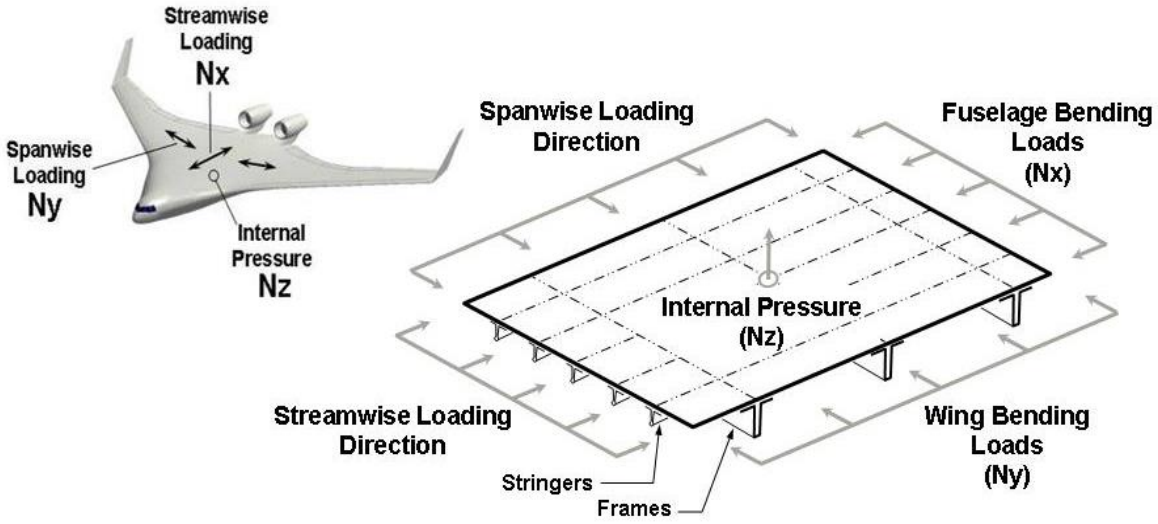

Figure 2. HWB pressure cabin crown panel loading.

The overall goal of the effort was to demonstrate that the PRSEUS concept can meet the demanding requirements of the next generation airframe technology. A key element of this effort was the recently completed testing performed at the Combined Loads Test System (COLTS) facility[19] located at the NASA Langley Research Center (LaRC). To demonstrate the viability of the PRSEUS concept, the design of a large test article was undertaken by the ERA project.[10,14,17] The assembly drawing of the test article is shown in Fig. 3. The test article was representative of an 80%-scale center section of a HWB 410,000 lb. maximum take-off weight aircraft[7] and, therefore, was suitable for structural performance evaluation under a combined loading environment where the multi-axial in-plane loads are combined with internal pressure loading.

The HWB center section test article was approximately 30 feet in span, 14 feet tall, and 7 feet deep. The exterior shell and floor comprised 11 PRSEUS panels, and the interior ribs comprised four composite sandwich panels. As shown in Fig. 3, the 11 PRSEUS panels were: one crown, one floor, one center keel, two side keels (left and right), two upper bulkheads (forward and aft), two lower bulkheads (forward and aft), and two outer ribs (left and right). The crown, floor, center keel, side keel, and outer rib panels were each stiffened by three equally-spaced frames oriented in the XZ plane and the stringers oriented perpendicular to them (i.e., along the Y-axis). The upper and lower bulkhead panels had their frames oriented in the vertical direction (i.e., along the Z-axis), while their stringers were oriented in the horizontal directions (i.e., along the X-axis). The four sandwich panels were two upper inner ribs (left and right) and two lower inner ribs (left and right) in the YZ plane. PRSEUS panels featured integral T-caps located near the panels' edges. T-caps, together with metallic fittings and fasteners, were used to join the panels in the assembly process. The scalloped contours of T-caps can be seen in Fig. 3 on the longer (forward) edges of the crown and keel panels.

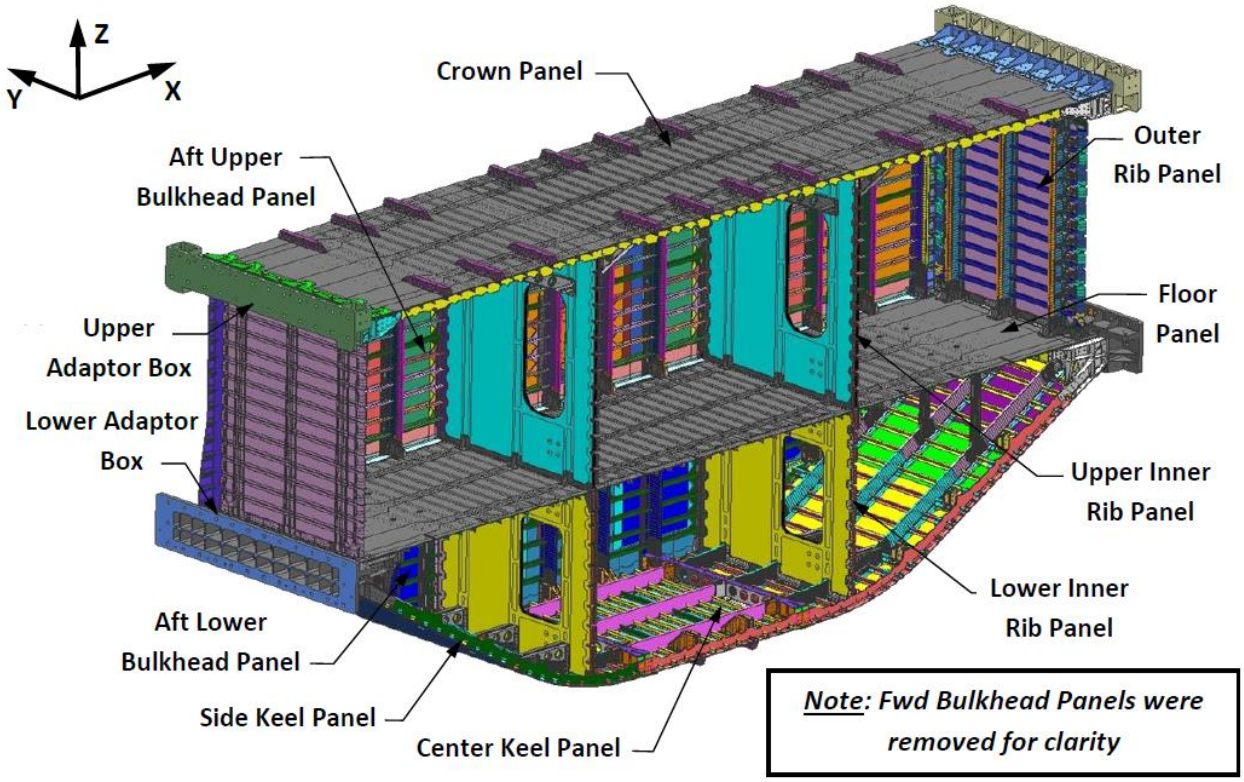

Figure 3. HWB center section test article assembly drawing.

II. Predictive Analysis and Test

The main objective of the analytical component of the overall activity was to develop a reliable analysis approach applicable to a HWB configuration built using the PRSEUS concept. This effort involved evaluation of both linear[18,20,21] and nonlinear[18,20,22] finite element analyses (FEA), including their computational efficiency and accuracy. While the initial studies were purely computational,[20,21] the present work benefits from the ability to validate predictions by comparing them to the test results. The studies performed for the pristine condition of the test article are discussed in detail in part I of this paper.[18] This paper (part II) discusses the predictive analysis and testing of the HWB center section article with inflicted severe damage, referred to also as the discrete source damage (DSD). Selection of the critical load and the DSD are discussed first in this section, followed by the description of the finite element model (FEM) and the FEA. Finally, the instrumentation used in the test is briefly introduced.

A. Discrete Source Damage and Critical Load

Based on the nonlinear FE analysis[22] and tests of the pristine HWB center section test article,[18,20] the three most critical load cases out of the five considered were identified as 2.5-g (wing up-bending), 2.5-g + 1P (wing up-bending plus internal cabin pressure), and 2P (internal cabin pressure-only, also called the overpressure condition). The most critical locations for the above three load conditions were either the crown panel or the upper bulkhead panel. Since the severity of the damage under consideration would preclude internal pressure containment in actual airframe, the most critical combination of the 2.5-g load and the DSD to the strongly compressed crown panel was chosen. Within the crown panel, the most critical structural members under the 2.5-g load were the three frames and two T-caps (forward and aft), carrying the majority of the compressive loads. No previous smaller scale tests of PRSEUS structures considered a configuration with severed frame or T-cap, so locating DSD at one of those locations was

desired. Due to symmetry considerations, the center frame and its surrounding area was chosen for the location of the DSD, as shown in Fig. 4.

Severing the center frame and the surrounding area effectively eliminated a critical load path in the panel. The extent of the damage in the Y direction was chosen to be 24 in., i.e., skin mid-bay to mid-bay. A preferred DSD location along the X-axis would be exactly at the mid-span of the crown panel, however, a stringer present at this location motivated moving the center of the DSD 3 in. from the centerline, as shown in Fig. 4. The 3 in. shift from the mid-span placed the DSD half-way between two consecutive crown panel stringers, since they were spaced 6 in. apart. The largest width of the DSD at the panel surface was 1 in. at the center frame location, and the center frame cut was additionally slanted to create 4.2 in. clearance at the frame depth. The above configuration was devised to preclude the DSD closure under the compressive load. The DSD width at the panel surface was linearly decreased toward the cut tips, which were 0.25 in. diameter. The bottom view of the crown panel skin cut and the side view of the crown panel center frame cut are shown as insets in Fig. 4. After completing the tests in pristine and barely visible impact damage (BVID) conditions, the DSD was applied to the crown panel without removing the test article from COLTS. A photograph of the DSD taken from the inside of the test article is shown in Fig. 5.

B. Finite Element Model and Analysis

The DSD test was added to the test plan late during the project, thus, only limited time was available to develop a corresponding FEM and conduct the predictive analysis. Given the constraints of the program schedule, the decision was made to limit the predictive FEA effort only to the global strength and stability analysis. No attempt was made to perform a progressive damage analysis. Consequently, the FEM of the pristine test article, discussed in more detail in part I of this paper,[18] was used as the basis of the DSD model. To recap briefly, shell elements were used to represent the composite panels and metallic fittings of the test article. The top sections of the frames and the pultruded rods in panel stringers were represented by beam elements. Connector elements were used to model metallic fasteners. The loading fixtures of the COLTS facility were modeled using a combination of shell and beam elements. The loads and boundary conditions are annotated in Fig. 4 and illustrate the 2.5-g mechanical load introduction.

The modifications of the pristine model in the span-wise (or Y) direction were confined to the area between the two consecutive stringers in between which the DSD was located, as shown in Fig. 4. In the direction along the stringers, the FEM modifications were confined between the forward and aft frames. After modeling the geometry of the DSD itself, the proximity of the DSD was meshed using significantly smaller shell elements when compared to the rest of the FEM where the typical element edge size was between 0.9 in. and 1.0 in. The smallest shell elements at the tip of the saw-cut were approximately 0.025 in. along the circumference of the tip by 0.05 in. across. The element edge size gradually increased away from the saw-cut tip up to 0.25 in., i.e., approximately one-fourth of the typical element size used in the pristine FEM. The refined area was joined with the coarser mesh away from the DSD using Nastran RSPLINE functionality,[23] which uses spline curves to interpolate displacements between mesh regions with dissimilar node grids.

The DSD test was intended to be carried out until a catastrophic damage of the test article occurred. While the airframe certification standards for a transport category airframe[24] require structure with DSD to support 70% of the design limit load (DLL), some airframe manufacturers apply a more conservative value of 100% DLL. Thus, the FEA with DSD was initially executed up to the 2.5-g DLL. Since the 2.5-g DLL analysis indicated, as it will be demonstrated in section III, that a catastrophic damage should not occur up to this load, an additional analysis was conducted up to the 2.5-g design ultimate load (DUL), where DUL is equal to 150% of DLL[24] (thus, 2.5-g DUL is equal to 3.75-g). While the DUL analysis also did not predict a catastrophic failure, the frame and T-cap results approached their allowable values (provided in Refs. 21 and 22). Consequently, no analysis beyond DUL was conducted, as the value of such an analysis was deemed limited without progressive damage analysis.

The FEA strains at the saw-cut tips were large enough to conclude that some local skin damage in the vicinity of the DSD will be developing even below the DLL. Consequently, the localized load redistribution was not being accounted for in the FEA. As these incremental damages would continue to develop and grow, the confidence in the analysis results was expected to gradually diminish.

A nonlinear static solver available in the commercial FE code MSC Nastran[23] (solution 400) was used to obtain the results presented in this paper. In addition, some selectively presented linear analysis results were obtained using solution 101. Material properties used in the analysis are the same as those presented in Ref. 22.

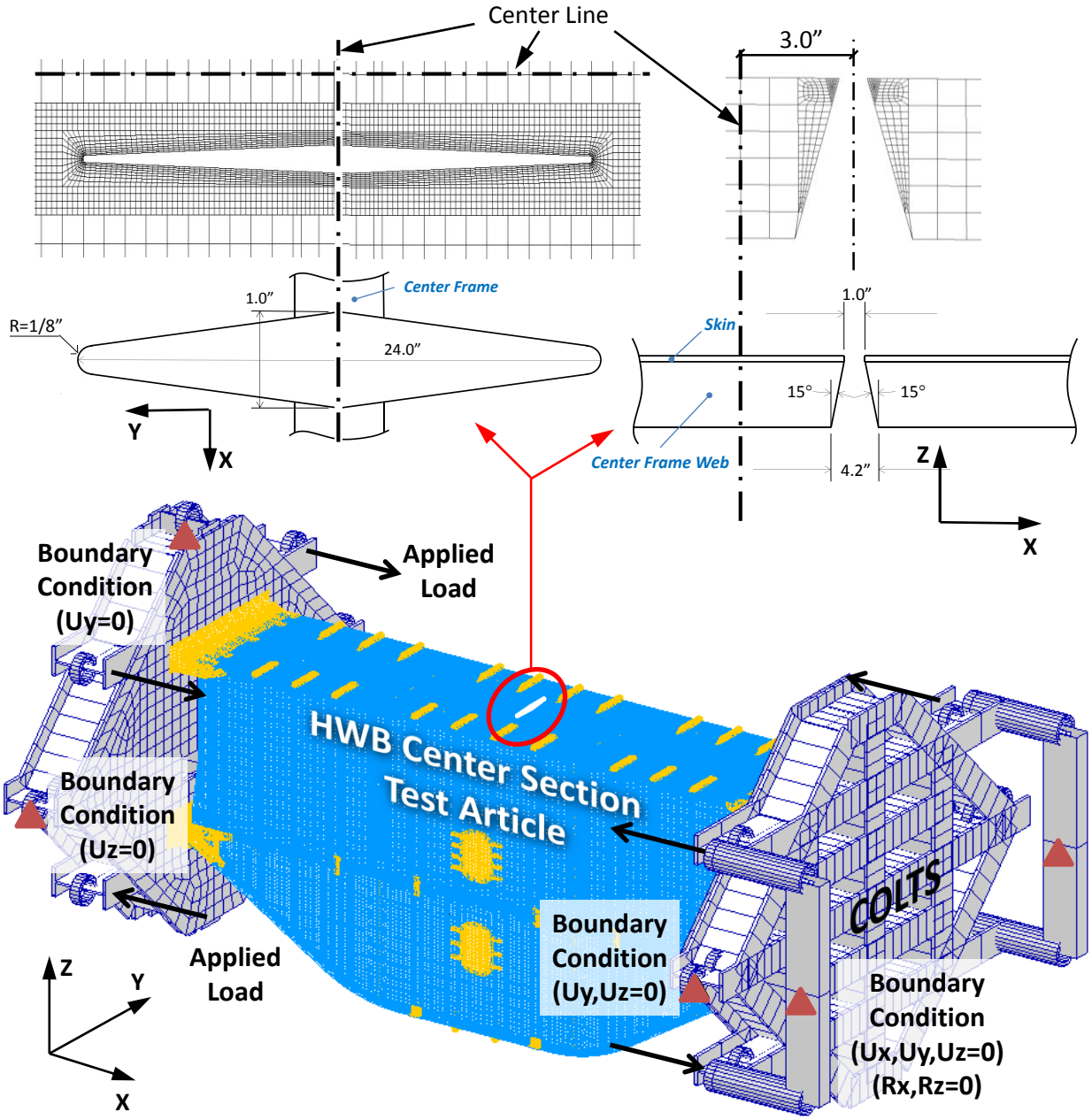

Figure 4. Finite element model of the test article with the crown panel saw-cut and COLTS test fixture (insets not to scale).

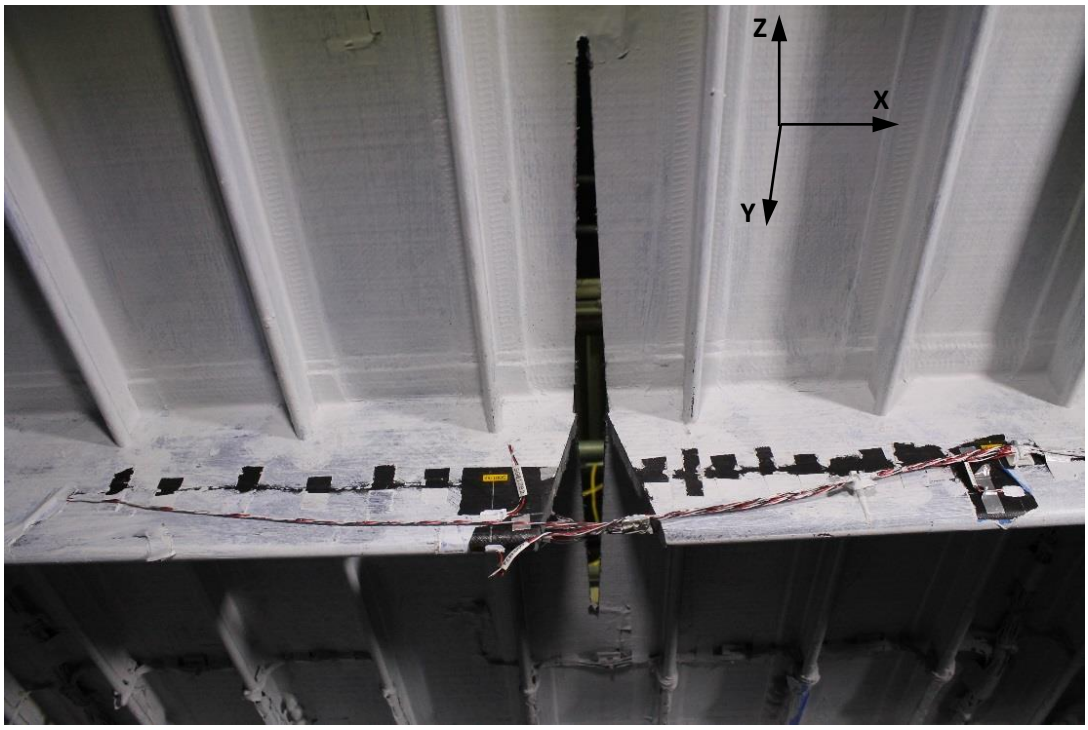

Figure 5. Crown panel saw-cut as seen from the inside of the test article.

C. Test Instrumentation

A large portion of the instrumentation devised for the pristine and BVID testing[18] was used in the DSD test. The video image correlation in three dimensions[25] (VIC-3D) acquisition system on the upper bulkhead panel remained unchanged relative to the previous tests, however, some of the crown panel measurements were conducted differently. Since the final damage was predicted to occur in the direct vicinity of the DSD, the global VIC-3D crown system was refocused on this smaller section of the panel, permitting higher-resolution measurements. Additionally, two local VIC-3D systems, set up with even higher resolution than that of the global system, were focused on small areas at both saw-cut tips. Since the center keel panel was not a critical location in the DSD test, the VIC-3D systems from the center keel panel used in the pristine and BVID tests were relocated to serve as the two afore-mentioned local systems on the crown panel. All the strain gauges not affected by the DSD were retained and several new gauges were added around the DSD on the inner moldline (IML) side of the crown panel. The reminder of this section focuses heavily on the crown panel VIC-3D and strain gauge results. Some of the upper bulkhead results are also discussed. The behavior of other panels was inconsequential to the final outcome of the test and, therefore, is omitted for brevity. Fiber optics strain results and acoustic emission measurements are documented in Refs. 26 and 27, respectively. A stand-alone report is also dedicated to the non-destructive evaluation of the test article, including before and after the final failure test.[28]

III. Results

The pre-test decision not to carry out the FEA beyond 2.5-g DUL, described in section II.B, was substantiated by the final test results.[29,30] While the initial localized damages at the tips of the skin saw-cut were noted at 130.3 kips actuator load (or 81.9% DLL), the final failure did not occur until an actuator load of 241.8 kips (152.1% DLL), i.e. just 1.4% above the DUL level up to which the nonlinear FEA was performed. Additional damages, as evidenced by strain gauge and VIC-3D measurements, occurred in between the first traceable damage initiation at 130.3 kips (81.9% DLL) and the final failure at 241.8 kips (152.1% DLL) within direct proximity of the DSD.

In the reminder of this section, the full-field VIC-3D out-of-plane displacement results on the outer moldline (OML) surfaces are introduced first at both DLL and DUL levels. The strain gauge results as a function of the actuator load are shown next for selected locations on both OML and IML surfaces. Displacement plots, introduced first, are used later to define general locations where the strain gauge data are compared with the FEA predictions (the locations are designated with letters repeated later in the strain figures). Insets showing schematics of a specific strain gauge placement are included in the strain figures (for the unidirectional gauges their colors match the colors of test curves). Strain gauge numbers, consistent with all other test documentation,[20,29,30] are included in the strain gauge plots. For the unidirectional gauges, their numbers are shown directly in plot legends. Since including much longer rosette numbers was not practical within the plot legends, their designations are included in figure captions. The designations of the IML crown panel gauges added for the DSD testing begin with 'sg19.' The predictive linear and nonlinear FEA results are shown up to DUL actuator load of 238.5 kips (150% DLL), while the test results are shown up to the final failure actuator load of 241.8 kips (152.1% DLL).

A. Displacements

The out-of-plane deformation of the crown panel with DSD under DLL is shown in Fig. 6, and under DUL in Fig. 7. The out-of-plane deformations of the aft upper bulkhead panel for the same two loads are shown in Figs. 8 and 9, respectively. The overall out-of-plane displacement characteristic of the crown panel shown in Figs. 6 and 7 is not significantly changed when compared to the results obtained without the DSD.[18,20] The deformation pattern is still dominated by the buckling of individual skin bays (i.e., sections of the skin between consecutive frames and stringers), including those with the saw-cuts. With the exception of the skin bays affected by the saw-cut, the overall displacement magnitudes are also similar (reference Fig. 21 in Ref. 18). The FEA results differ from those measured during the test primarily due to differences in which skin bays buckled inward and which buckled outward. Specifically, it is seen that during the test, the saw-cut skin bay located aft the span-wise centerline in Figs. 6 and 7 buckled outward and this measurement is matched by the FEA results. However, the saw-cut skin bay located forward of the span-wise centerline in the same two figures buckled inward and this result is not matched by the FEA analysis. As discussed in sections III.A and III.D of Ref. 18, individual skin bays under compression have a potential to adopt one of the two stable equilibria. Which one of the two is actually realized depends on imperfections in the structure that are not considered in the FEA that is based on the nominal dimensions and on the assumption that the structure is completely stress free when no external load is applied. Thus, the saw-cut bay behavior is not unique when compared with the previously discussed results without the DSD.[18] Furthermore, for the specific skin bay in question, the technicians who worked on imparting the DSD reported that once the saw-cut was made, they observed a slight tendency of this particular skin bay to display an inward displacement bias even in a load-free condition. This observation further confirms the validity of geometrical imperfection and/or residual stress condition being responsible for the differences observed between the test and FEA results in the skin bay areas.

The overall out-of-plane displacement characteristic in the top section of the upper bulkhead panel, shown in Figs. 8 and 9, is also not significantly changed when compared to the results obtained without the DSD (reference Fig. 25 in Ref. 18). The deformation pattern is still dominated by the buckling of individual skin bays, with the same characteristic pattern of multiple skewed semi-sine-like shapes within individual skin bays. The range of displacement magnitudes for the pristine and DSD crown panel conditions is also comparable.

For the crown and upper bulkhead panels, a good qualitative comparison between the FEA and test out-of-plane deformations is obtained, with the FEA results showing slightly smaller displacement magnitudes, especially for the upper bulkhead panel under the DUL. This result was expected as the test article was softened due to damage, thus it deformed more for a given load, and that softening was not replicated in the FEA.

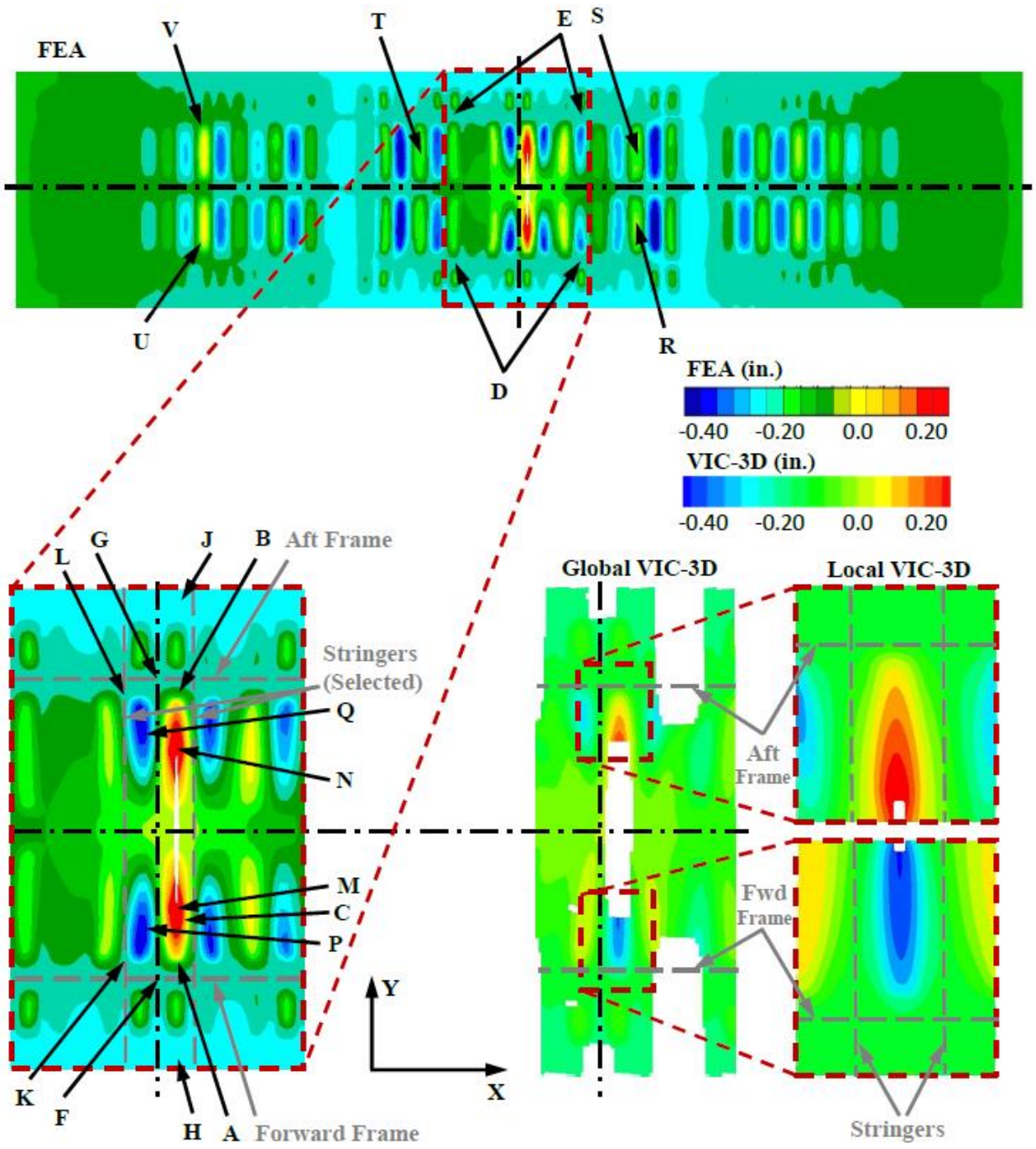

Figure 6. Out-of-plane deformation of the crown panel with DSD under DLL (the locations of strain gauges to be discussed labeled alphabetically).

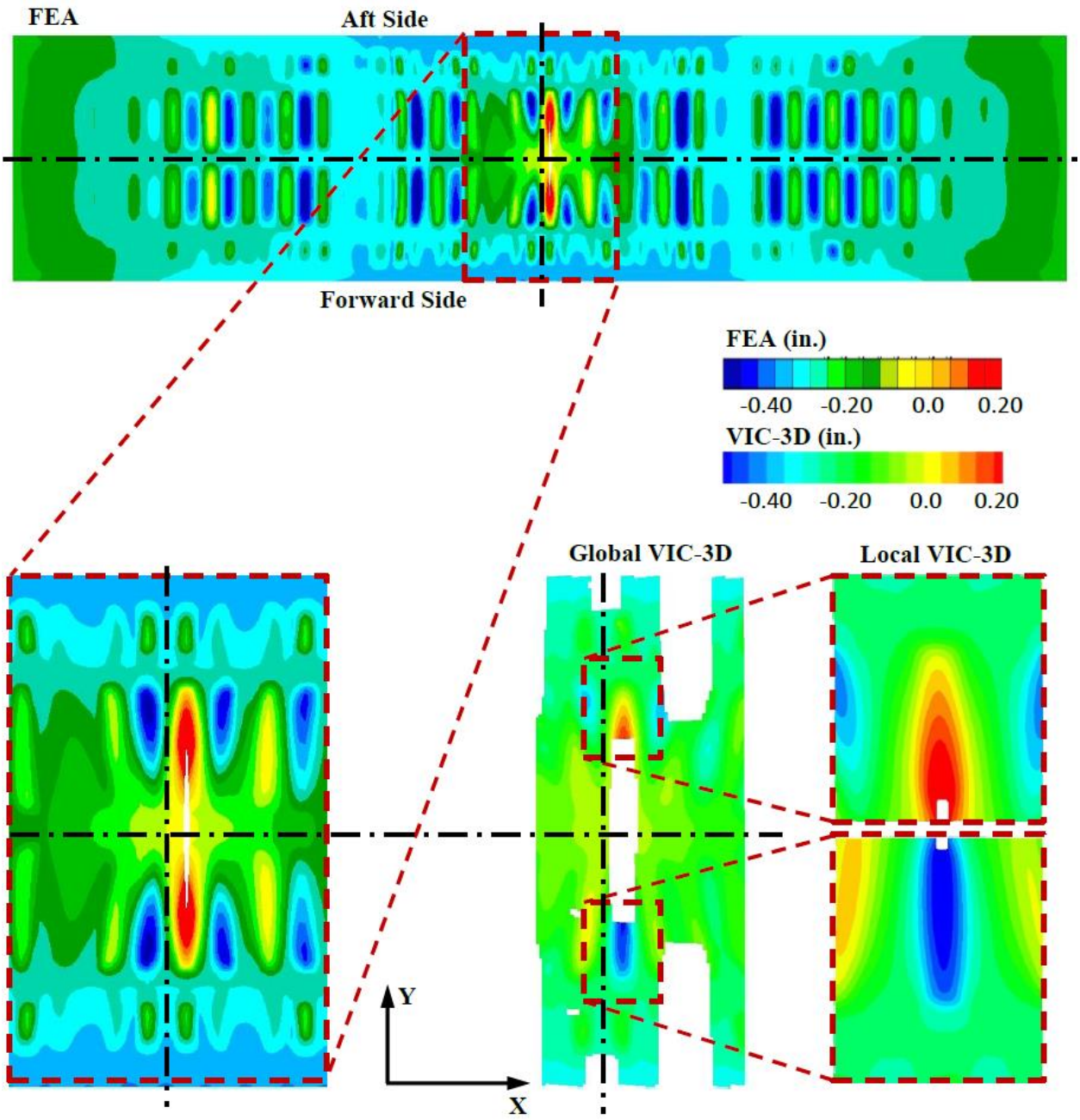

Figure 7. Out-of-plane deformation of the crown panel with DSD under DUL.

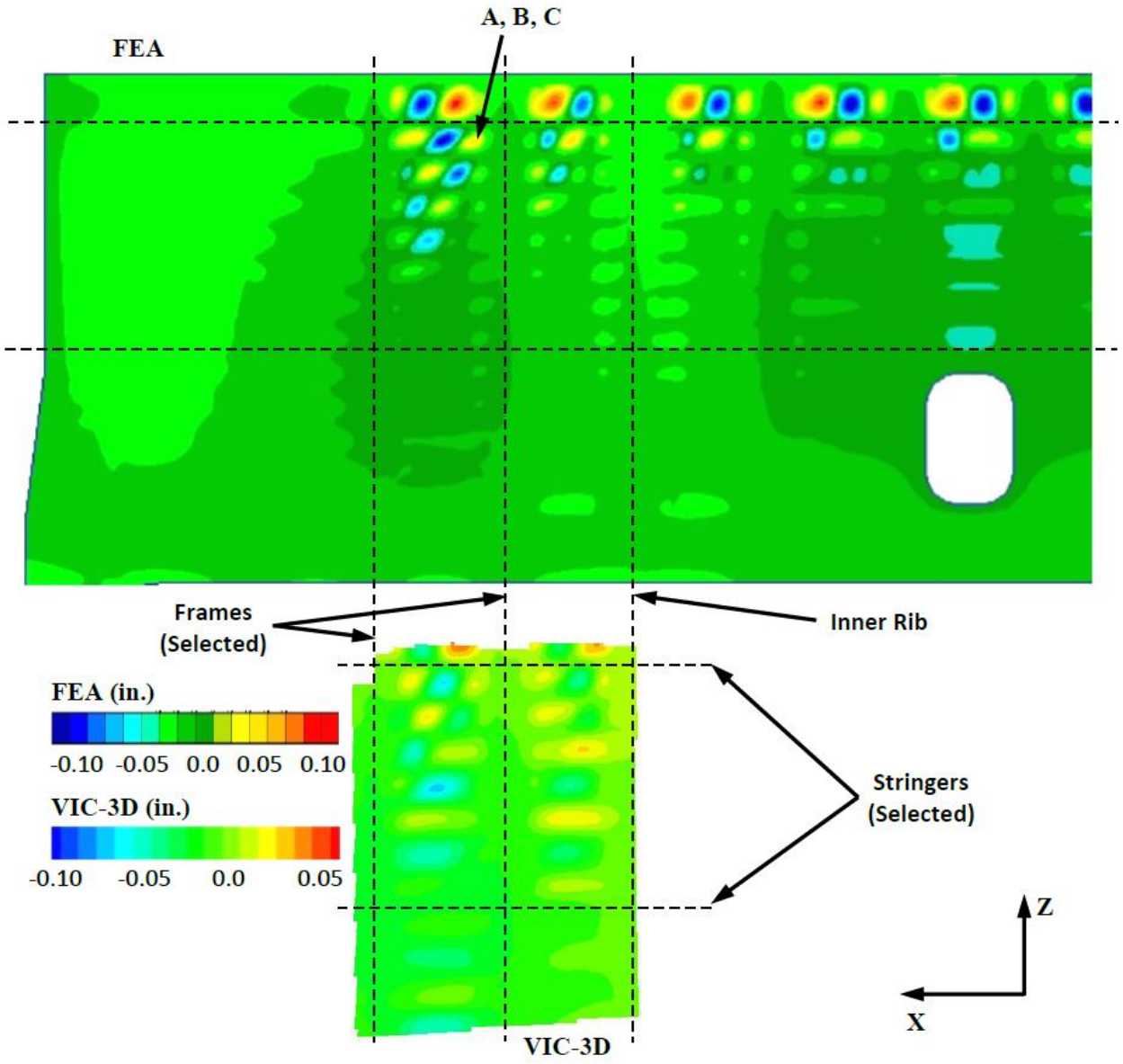

Figure 8. Out-of-plane deformation of the upper bulkhead panel with the crown panel DSD under DLL.

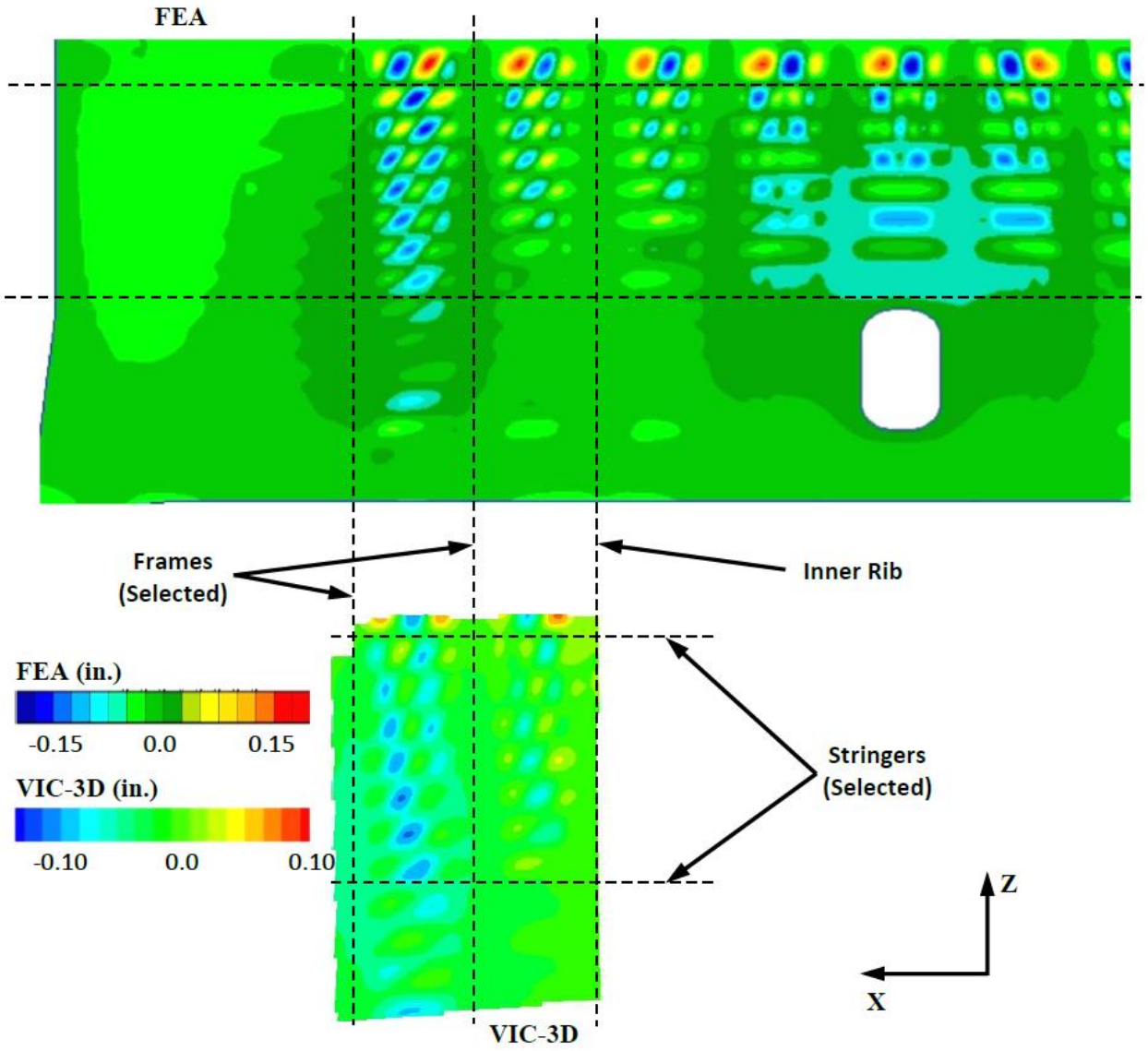

Figure 9. Out-of-plane deformation of the upper bulkhead panel with the crown panel DSD under DUL.

B. Strains

The strain results in the forward frame flange, i.e., in the vicinity where the final failure likely originated, are shown in Fig. 10. The largest recorded compressive strain of −0.007938 in./in. in the crown panel substructure just before the final failure is seen in this plot. The two strain gauges shown in Fig. 10 are located on the side of the DSD where the skin buckled in the direction opposite to that predicted, see location A in Fig. 6. Thus, the nearby forward frame flange was also affected by this behavior and, consequently, the FEA and test results correspond to two distinct buckled equilibria. This conclusion is supported by the strain results shown in Fig. 11, i.e., on the side of the DSD where the predicted and test results both showed outward buckling. While the agreement between the predicted and test results shown in Fig. 11 is not perfect, it is noticeably better than that of Fig. 10. The discrepancy between the prediction and test results seen in Fig. 11 can be, at least in part, attributed to the presence of several panel thickness discontinuities in the vicinity of the two gauges that are introduced by the intersection of the frame and stringer flanges. In addition, the FEM mesh resolution was not adequate to capture accurate strain gradients at the locations of the thickness changes.

In general, since the initial local damages at the saw-cut tips were noted at 130.3 kips (81.9% DLL) on the forward side and at 131.8 kips (82.9% DLL) on the aft side, their presence and progression could have also contributed to the degraded comparison at the higher loads (the test results evidencing local damages are presented later in this section).

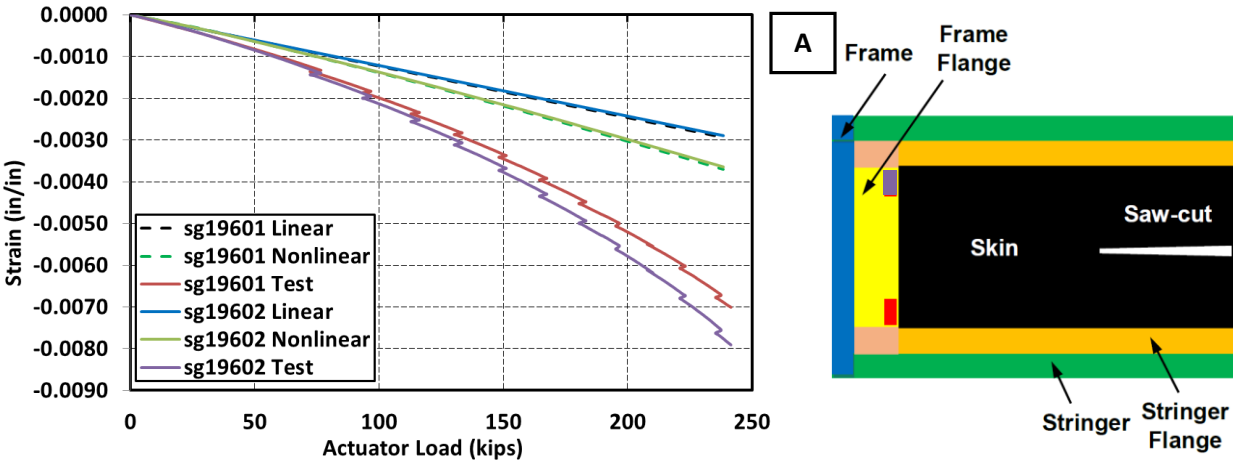

Figure 10. Forward frame flange strains in the vicinity of the DSD.

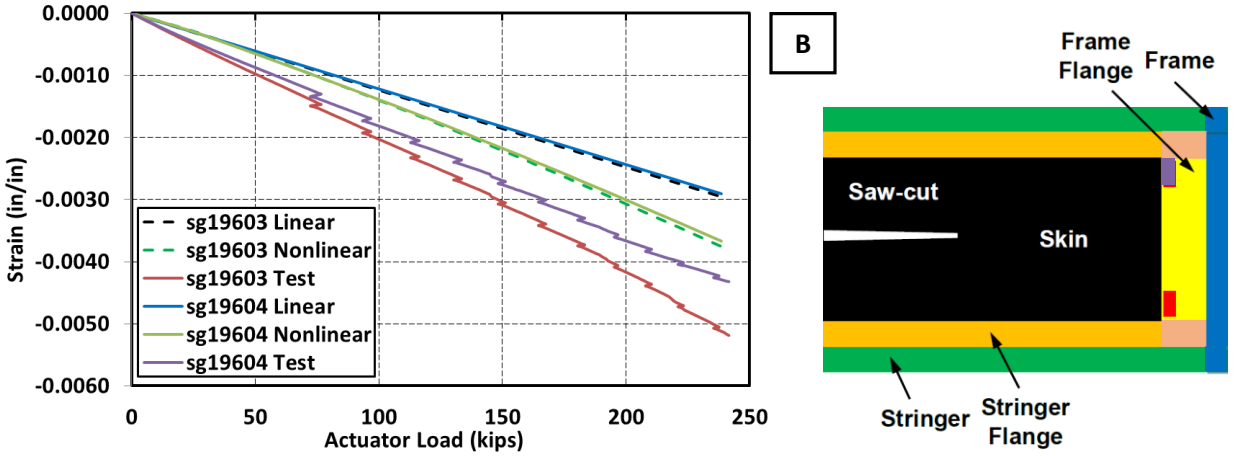

Figure 11. Aft frame flange strains in the vicinity of the DSD.

Strain results in the flanges of the two stringers in the vicinity of the DSD are shown in Fig. 12. Since the two gauges are affixed in the Y direction perpendicular to the span-wise X direction in which the main loads are carried under the 2.5-g condition, very low strain levels (not exceeding 0.00075 in./in.) are obtained. Comparison of very low strain levels is not particularly useful because of the level of accuracy of the gauges and load cells, so the difference in values between test and FEA is not a concern. The main purpose of installing the stringer flange gauges was to track potential damage progression originating from the saw-cut tips (they are installed on the ±45-degree directions extending from the saw-cut tips, which in other PRSEUS tests was found to be a common damage propagation path). It is seen in Fig. 12 that gauge sg19302, corresponding to location C in Fig. 6, is showing an event consistent with a localized damage progression at 207.7 kips (130.6% DLL). A different slope of the strain versus load curve after the event is indicative of a local change in stiffness of the surrounding structure. However, since the gauge continues to provide strain measurements above this load, it is concluded that the damage must have occurred in the vicinity of the

gauge but not directly at the gauge location. This observation is consistent with a local skin damage propagation being arrested at the stitch line of the stringer flange in the vicinity of the gauge.

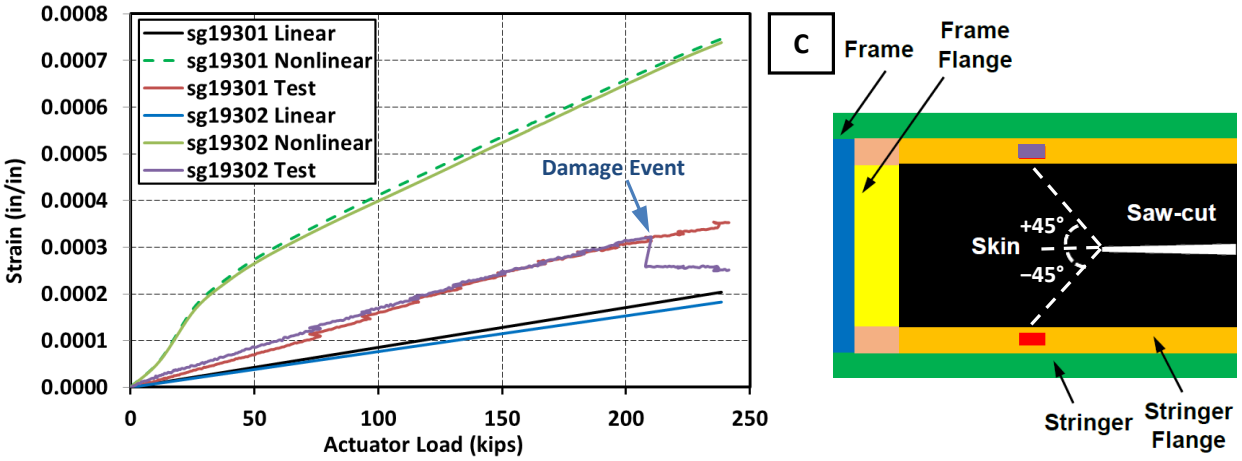

Figure 12. Stringer flange strains in the vicinity of the DSD.

The strain results at the tops of the forward and aft frames in the proximity of the DSD are shown in Figs. 13 and 14, respectively, and correspond to locations D and E in Fig. 6. The strains display moderately nonlinear characteristics reaching approximately −0.004 in./in. at DUL and, generally, the comparison between the FEA and test results is good (at DUL the predictions of gauges sg19801, sg19803, and sg19804 are off by 1.7%, 5.4%, and 1.2%, respectively, relative to the measured strains). The only gauge among the four symmetrical gauges in Figs. 13 and 14 that shows a slightly degraded comparison (11% off the measurement) is gauge sg19802 at the left location D in Fig. 6. This location corresponds to the same quadrant of the panel where the side frame flange gauge, sg19602, produced the largest substructure compressive strain, as presented in Fig. 10. This further substantiates the previous observation that the forward left quadrant of the panel, was the one that experienced the highest strains and where the final failure originated.

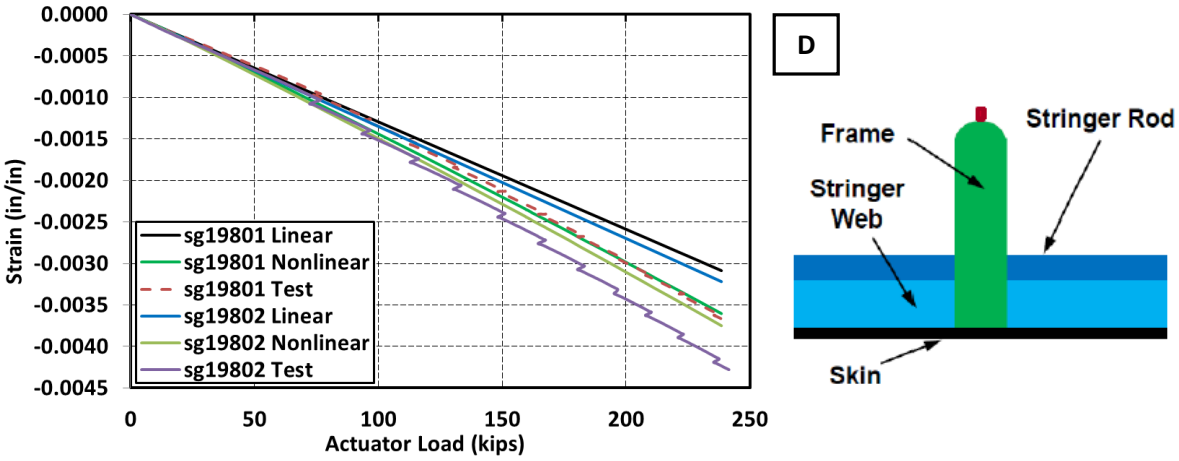

Figure 13. Strains at the top of the forward frame in the vicinity of the DSD.

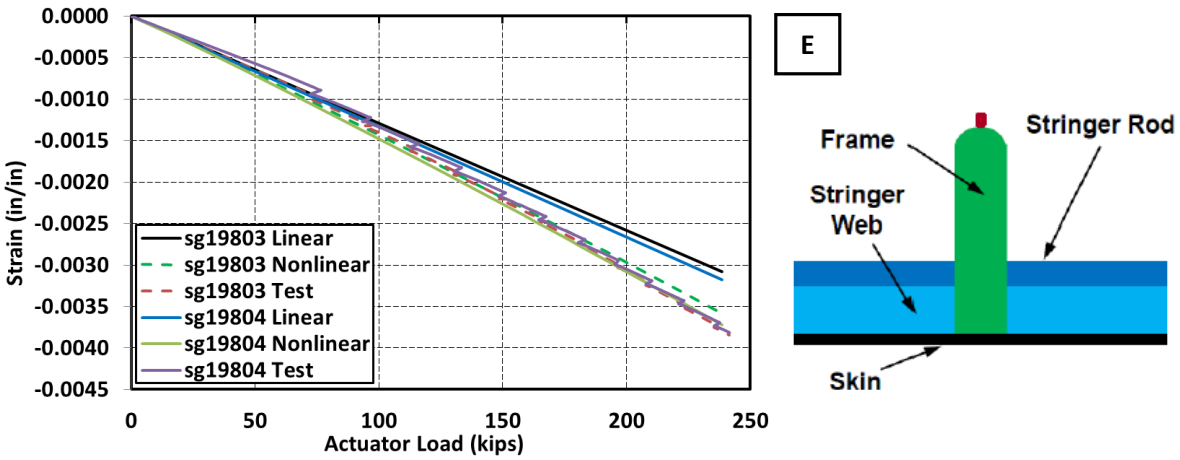

Figure 14. Strains at the top of the aft frame in the vicinity of the DSD.

The strain results on the webs of the forward and aft frames in the proximity of the DSD are shown in Figs. 15 and 16, respectively, and correspond to locations F and G in Fig. 6. The strains display moderately nonlinear characteristics reaching approximately −0.0035 in./in. at DUL and, generally, the comparison between the FEA and test results is very good (within 4.4% for all four gauges). What is more important, the strain levels on both sides of the two frame webs are very similar, thus it can be concluded that the frames are uniformly compressed across their thicknesses, and no meaningful sideways bending of the frames existed until the failure load was reached. This observation means that buckling of the side frames was not a factor and that they ultimately failed by exceeding strength capabilities rather than in the stability mode (i.e., by crushing rather than by buckling), which is a preferred failure mechanism and results in a higher load carrying capability.

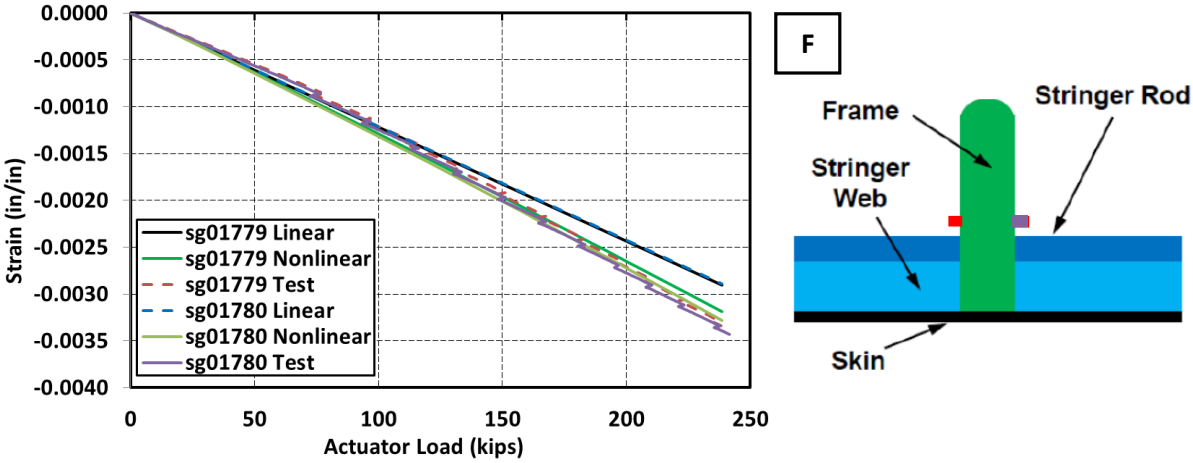

Figure 15. Side-to-side strains in the forward frame web in the vicinity of the DSD.

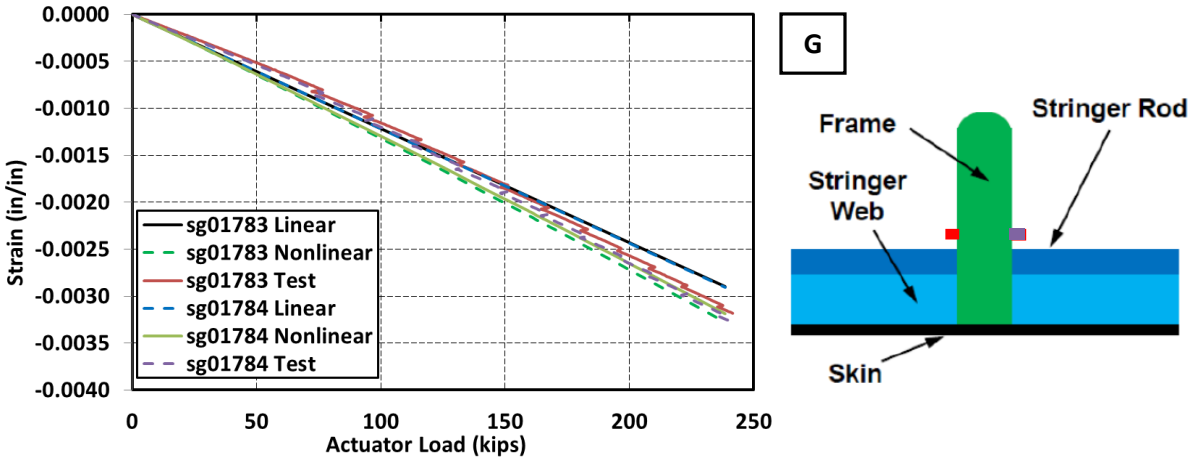

Figure 16. Side-to-side strains in the aft frame web in the vicinity of the DSD.

The strain results at the forward and aft T-caps in the proximity of the DSD are shown in Figs. 17 and 18, respectively, and correspond to locations H and J in Fig. 6. Both predicted and measured strains compare very well until they depart from the linear behavior at approximately 125 kips (79% DLL). Beyond that load, the predicted and actual nonlinear behaviors differ. The measured strains at DUL reach approximately −0.0033 in./in. on the forward side and −0.0038 in./in. on the aft side, and are larger than those predicted by 21% and 38%, respectively. While the predicted strains in the forward and aft T-caps were different, the actual test measurements differed by an even larger margin. Furthermore, in the results discussed thus far, the forward frame flanges (Fig. 10), tops (Fig. 13), and webs (Fig. 15) were typically showing slightly larger strains than those on the aft side (Figs. 11, 14, and 16, respectively). This trend is reversed in case of the T-caps, where the aft T-cap at failure shows a larger compressive strain than the forward T-cap. The reason for this behavior was not conclusively established.

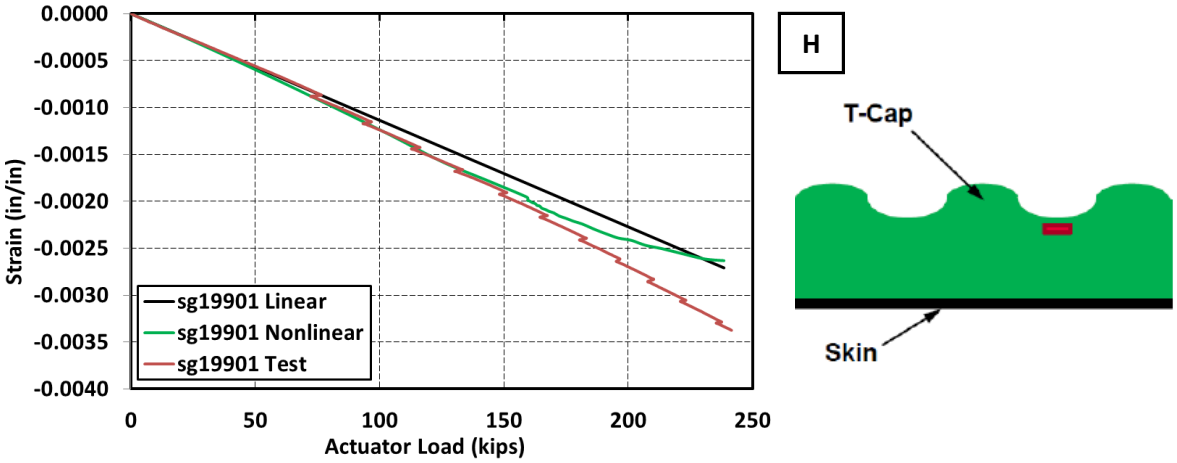

Figure 17. Strains in the forward T-cap in the vicinity of the DSD.

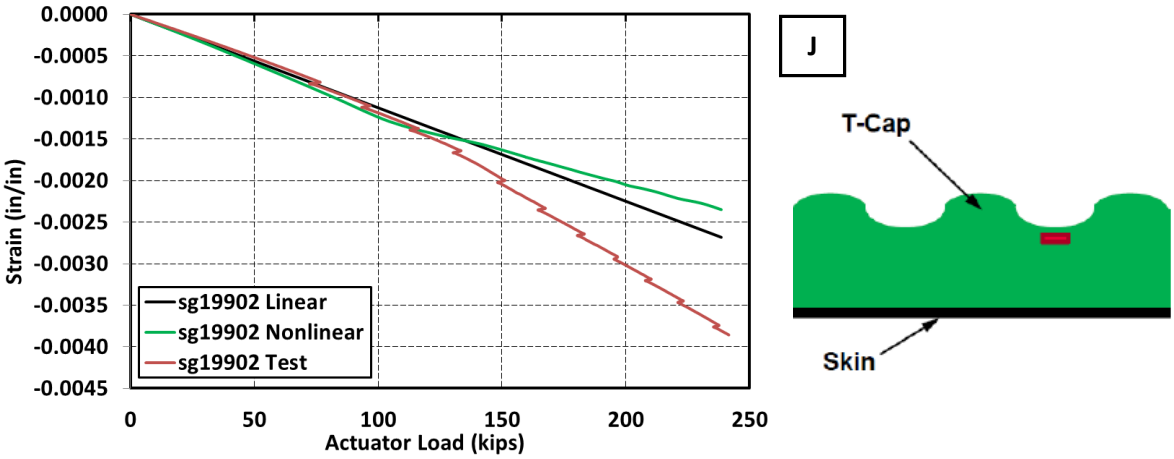

Figure 18. Strains in the aft T-cap in the vicinity of the DSD.

The principal strain results at the webs of the stringer in the proximity of the DSD are shown in Figs. 19 and 20, and correspond to locations K and L in Fig. 6, respectively. The two locations are in the vicinity of the stringer intersection with the forward and aft frames. The strains do not exceed 0.001 in./in. at the failure load. Such low principal strain levels are consistent with the orientation of the stringer in the direction perpendicular to the main span-wise load path. The strains display slightly nonlinear characteristics, thus the nonlinear solution compares better with the test results than the linear solution. Since the strain gauges in Figs. 19 and 20 are placed very close to the frame-stringer intersections, a factor that might have influenced the comparison was the approach taken to model these intersections. The FEM was created based on the assumption that the bonds between the frames and the stringers are a byproduct of the manufacturing process, as they were not designed to serve as fully bonded joints. Consequently, the frame-stringer intersections were modeled as completely independent surfaces that do not share nodes and are not connected otherwise. This modeling assumption warrants further investigation.

Upon closer examination, it is seen in Figs. 19 and 20 that both minimum and maximum strains show discontinuities. For the location near the forward frame intersection, these discontinuities are seen at 189.8 kips actuator load (119.4% DLL) and for the location near the aft frame intersection at 218.3 kips actuator load (137.3% DLL). The strain discontinuities are indicative of the damage developing in the proximity of the DSD, but most likely not in the subject stringer, as evidenced by otherwise smooth and continuous strain characteristic after the strain discontinuities are encountered.

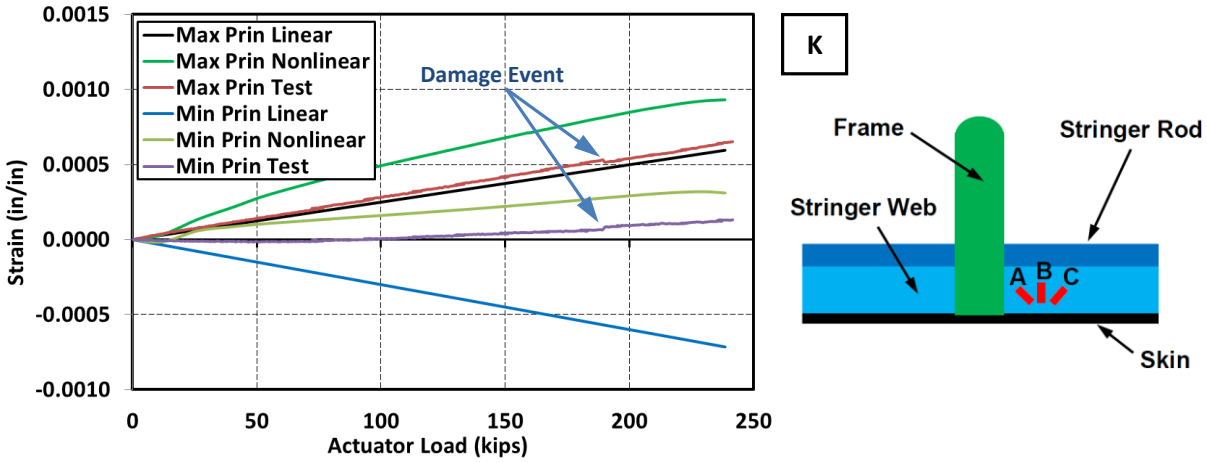

Figure 19. Principal strains in the stringer web near the forward section of the DSD (sg01426A/sg01427B/sg01428C).

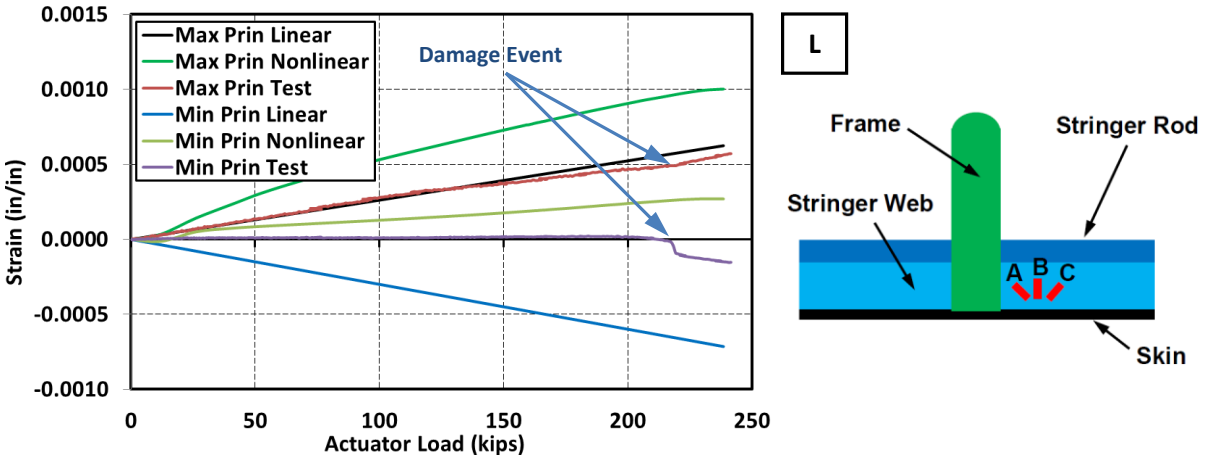

Figure 20. Principal strains in the stringer web near the aft section of the DSD (sg01430A/sg01431B/sg01432C).

As briefly mentioned at the beginning of this section, the first evidence of damage in the vicinity of the DSD was noted at 130.3 kips actuator load (81.9% DLL). The two strain gauge measurements taken at the tip of the forward side of the saw-cut are shown in Fig. 21. The strain gauge located closer to the saw-cut tip fails at the afore-mentioned load indicating damage at this location. The second gauge, further away from the saw-cut tip, fails soon thereafter at 154.0 kips (96.9% DLL). Such a behavior is indicative of the damage directly affecting the site where the two strain gauges were installed.

The FEA results and test measurements shown in Fig. 21 do not agree well. This is due to the fact that, per discussion of the out-of-plane displacement results in Figs. 6 and 7, the skin bay on the forward side of the DSD buckled in the inward direction, i.e., opposite to the outward direction predicted by the FEA.

A similar damage development sequence to the one described on the forward DSD side was also observed on the aft side of the DSD, as shown in Fig. 22. The strain gauge closer to the saw-cut tip fails at 131.8 kips actuator load (82.9% DLL), i.e., just 1.5 kips (less than 1% DLL) above the symmetric gauge on the forward DSD side. The damage to the area where the second gauge was installed slightly further away from the saw-cut tip can be noted at 173.1 kips actuator load (108.9% DLL). Since the aft side saw-cut skin bay buckled in the direction predicted by the FEA, the agreement between the test and analysis is much more favorable when compared to Fig. 21.

The strain gauges on the forward side of the DSD failed at a higher tension strain levels when compared to the magnitudes of the compressive strains on the aft side gauges. This behavior is consistent with the typical composite system strength performance, where the compression design values are lower than the tension design values.

All four actuator loads associated with the saw-cut tip damage intiation and progression shown in Figs. 21 and 22 are of lower magnitudes than those discussed for the stringer web strain gauge discontinuities shown in Figs. 19 and 20. Thus, it can be concluded that the stringer web strain discontinuities are associated with a further damage progression and not with the initial damages at the saw-cut tips.

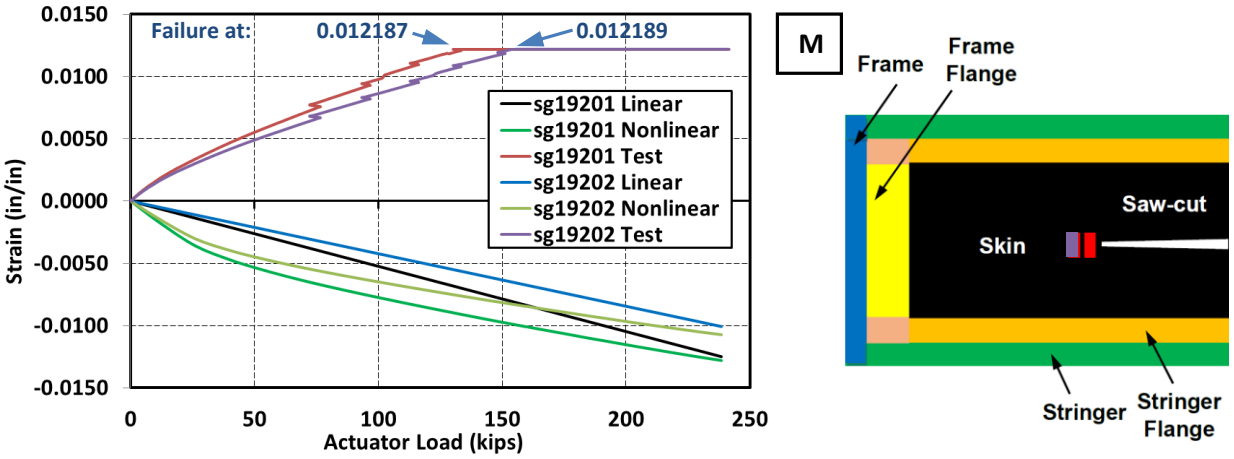

Figure 21. Strains in the forward section of the crown panel skin near the tip of the DSD.

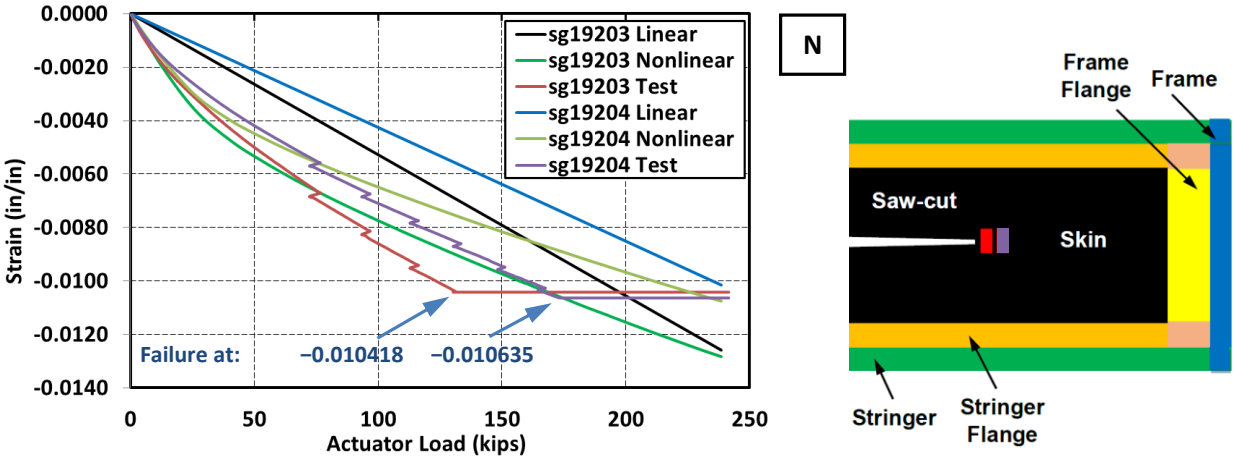

Figure 22. Strains in the aft section of the crown panel skin near the tip of the DSD.

The back-to-back strains in the skin bays next to the skin bays with the DSD are shown in Fig. 23 and correspond to locations P and Q in Fig. 6. It is seen that in location P the strain agreement would be favorable if the IML measurements were compared with the OML predictions, and vice versa (such a comparison would yield 29% and 31% errors, respectively). The results in Fig. 23 are consistent with the out-of-plane test displacements shown in Figs. 6 and 7. Since the skin bay with the DSD on the forward side shows the displacement opposite to that predicted, the next skin bay over on the forward side also adopts the displacement opposite to the one predicted. Thus, the strain sign reversals between the IML and OML surfaces.

Strain results at location Q of Fig. 6 are also shown in Fig. 23 and a favorable agreement between the FEA results and test measurements is seen at the lower load levels (at 79.5 kips actuator load or 50% DLL, the errors at OML and

IML surfaces are 21% and 6.9%, respectively). However, as the load increases the agreement deteriorates. It is likely a result of the damage progressing outwards from the DSD vicinity. While the entire skin bay does not snap through to the opposite equilibrium, the damage developing in the proximity of the DSD is likely causing the buckled skin shape to become distorted relative to that predicted and, consequently, for the strain comparison to deteriorate.

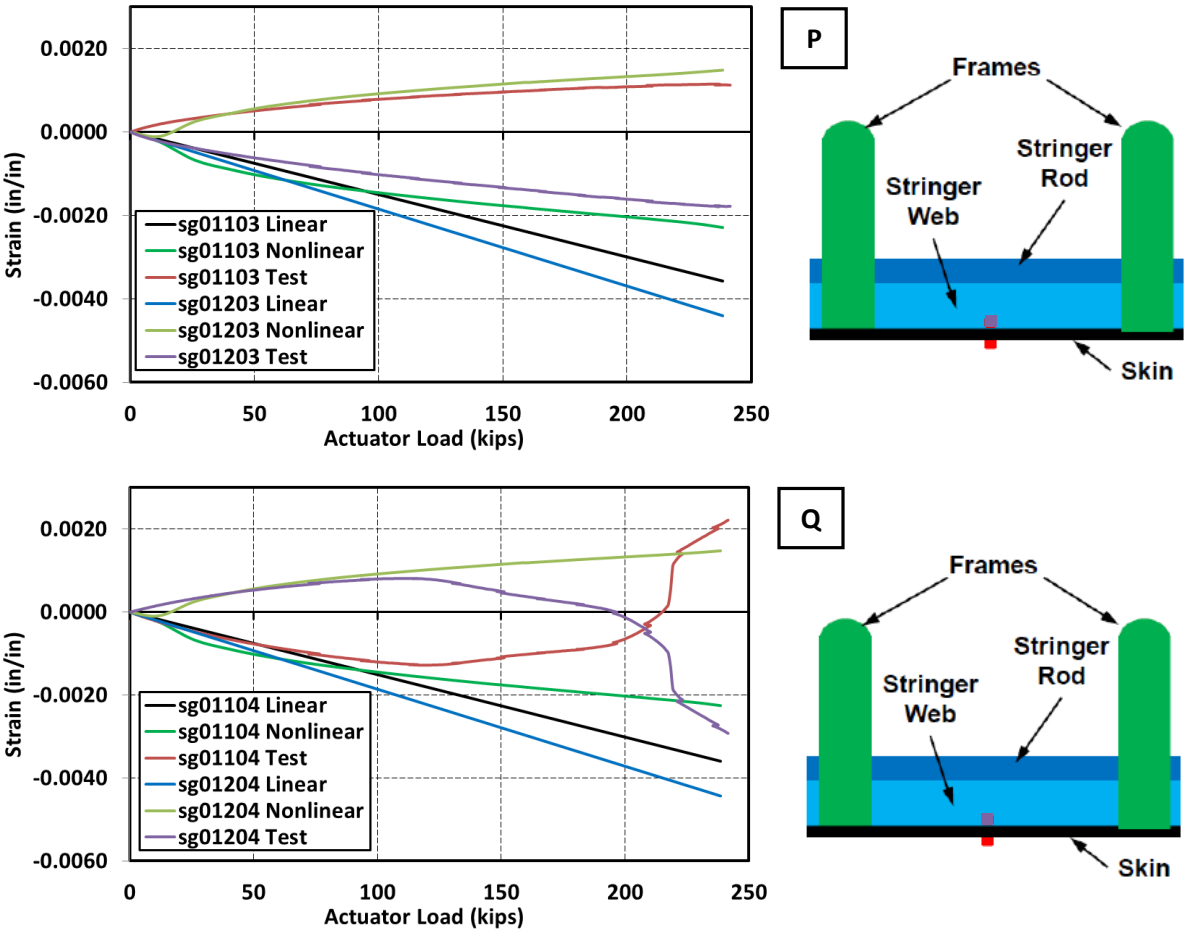

Figure 23. Crown panel back-to-back skin strains in the vicinity of the DSD.

The back-to-back skin strains in the skin bays further away from the DSD, relative to those of Fig. 23, are shown in Fig. 24 and correspond to locations R, S, and T in Fig. 6. Overall, a favorable comparison between the FEA results and test measurements is found for locations S (8.9% and 4.9% difference at DUL on the OML and IML side, respectively) and T (11% and 26%). These locations are on the aft side of the crown panel, which is the side where the buckling pattern agreed between the prediction and the test. Results at location R display test strains with the opposite sign relative to those predicted, i.e., the IML predictions fall close to the OML test results and vice versa. This behavior is due to the test buckling pattern being the opposite relative to the one predicted.

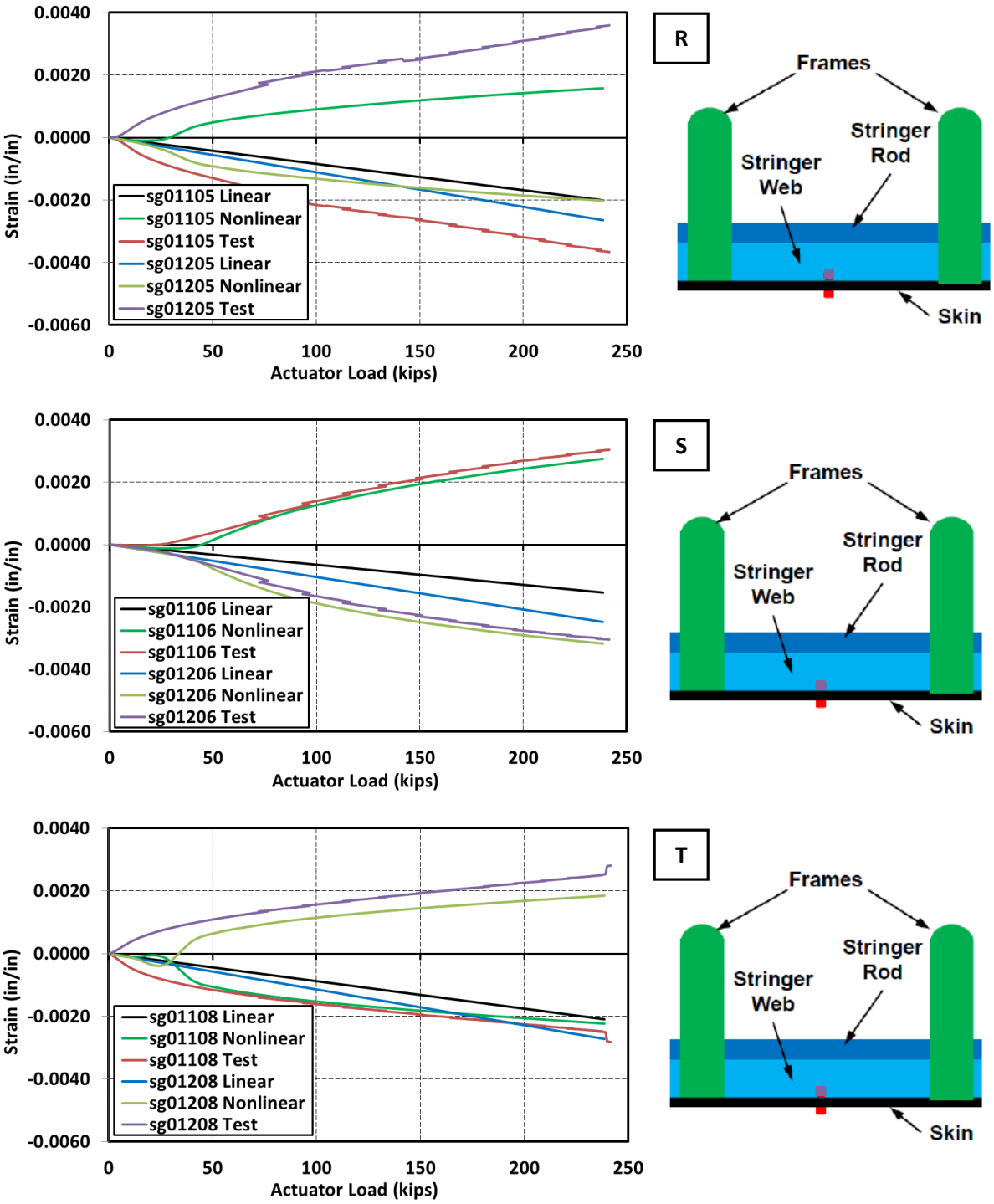

Figure 24. Crown panel back-to-back skin strains away from the DSD.

The principal skin strains in the skin bays in the side section of the crown panel are shown in Figs. 25 and 26, and correspond to locations U and V in Fig. 6, respectively. Favorable agreement between the FEA and test results is found at both locations (at DUL, the difference between the predicted and measured minimum principal strain is 17% at location U and 8.8% at location V). At both locations, that are distant from the DSD, the strain characteristics are

very similar to those obtained for the pristine crown panel condition (see Fig. 23 in Ref. 18 for the pristine strain results at location V).

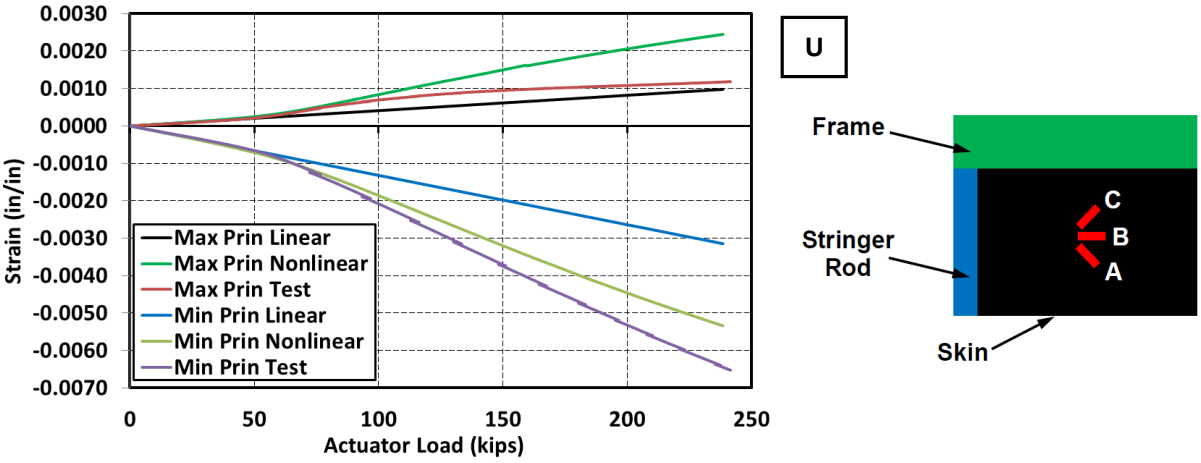

Figure 25. Principal strains in the crown panel skin (sg01287A/sg01288B/sg01289C).

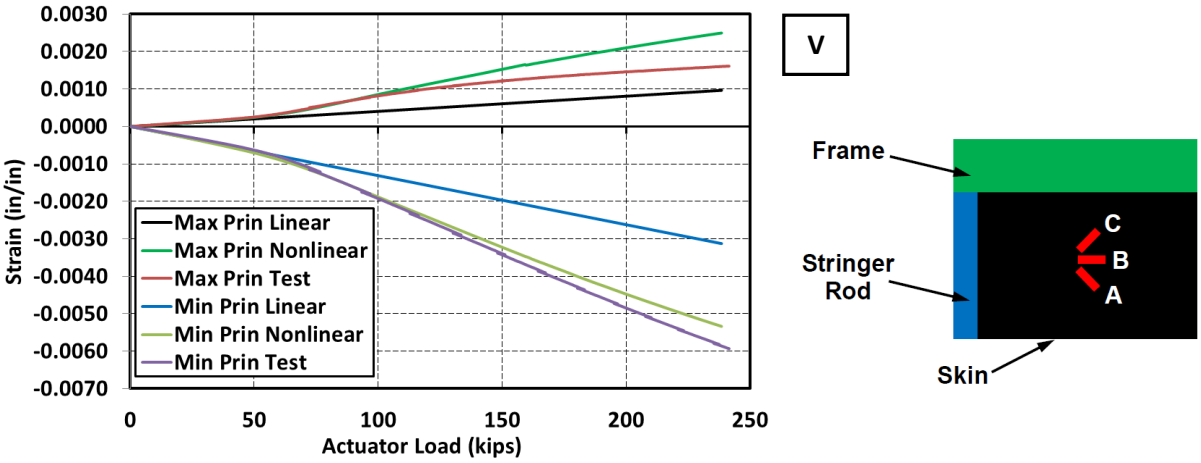

Figure 26. Principal strains in the crown panel skin (sg01290A/sg01291B/sg01292C).

To summarize the strain predictions for the crown panel with the DSD, the overall level of agreement was comparable to the pristine 2.5-g case[18] in the low range of the applied load, i.e., below the level where damages originating from the DSD began to develop. Several instances of test strain discontinuities stemming from the damage development and progression were noted at the following actuator load levels: 130.3 kips (81.9% DLL, shown in Fig. 21), 131.8 kips (82.9% DLL, Fig. 22), 154.0 kips (96.9% DLL, Fig. 21), 173.1 kips (108.9% DLL, Fig. 22), 189.8 kips (119.4% DLL, Fig. 19), 207.7 kips (130.6% DLL, Fig. 12), and 218.3 kips (137.3% DLL, Fig. 20). While the list of the actuator load levels where the events were identified is complete based on the recorded strain data, the list of gauges that are used to demonstrate them is selective. With that many incremental damages occurring over nearly half of the entire load range, certain discrepancies between analysis that does not support progressive damage and the test results can be expected. Thus, given the limited time to set up and execute the analysis with the DSD, as well as the size and computational complexity of the strongly nonlinear analysis with several sections undergoing buckling, the overall outcome of the analysis is considered favorable. The analysis was able to guide the selection of strain gauges and other instrumentation, such that a meaningful test data set was acquired.

The principal strains in the upper section of the skin of the upper bulkhead panel are shown in Fig. 27. Despite the fact that the FEA analysis predicted buckling in the upper skin sections of the bulkhead panel, as evidenced in Figs. 8 and 9, some of the skin bays achieved different buckled equilibria in the test. Consequently, skin strains in the upper bulkhead panel do not display good agreement in terms of both strain magnitudes and overall trends, especially at locations B and C. The crown panel buckling shapes of individual skin bays were typically resembling semi-sine shapes, so even if the buckled equilibrium opposite to that predicted was achieved in test, the OML strain predictions would resemble the characteristic of the IML measurements, and vice versa, as demonstrated at location T in Fig. 24. Since the buckling shapes of the top section of the upper bulkhead are more complex than those of the crown panel, the differences between predicted and actual buckling shapes do not result in a simple mirroring of the OML and IML strain characteristics.

IV. Concluding Remarks

The HWB center section proof-of-concept article was first tested in the pristine and BVID conditions under five different load scenarios. Successful completion of these tests enabled the final test to failure with the DSD inflicted to the critical load path of the crown panel under the 2.5-g wing up-bending load. The test article failed at 152.1% DLL (or 101.4% DUL), greater than the 70% of DLL required by the transport category aircraft certification standards and greater than some airframe manufacturers' more conservative 100% DLL requirement.

As indicated before, the final test to failure was added to the overall test plan late in the test planning stage, therefore, the extent and scope of the supporting analysis was limited by the program schedule. Once the DSD was incorporated into the FEM with a refined mesh in its proximity, the same type of nonlinear analysis was executed as previously performed for the pristine test article. No attempt was made to execute a progressive failure analysis. Consequently, the analysis generally produced accurate results until damage began to develop and propagate. After that point, the quality of the test-analysis correlation gradually diminished.

Similar to the pristine condition nonlinear FEA, the DSD analysis was also prone to locally predicting buckling shapes opposite to those realized in the test. Since the skin bays with the saw-cut tips buckled before the onset of the initial damage, one of the saw-cut skin bays buckled in the direction opposite to that predicted. While the reasons and the potential mitigation measures for this behavior are the same as the ones discussed for the pristine analysis, it has to be stressed that predicting the correct buckled equilibrium near the DSD is likely more consequential for the DSD analysis than it is for the pristine condition analysis. While, as stated in part I of the paper, quantifying and modeling initial geometric imperfections for the entire large FEM does not seem practical nor necessary, such extra modeling fidelity may be practical and warranted in the most direct proximity of the DSD.

Despite the above limitations, the DSD nonlinear FEA performed before the test was very useful in defining the geometry of the DSD and developing an instrumentation plan for the DSD test. The analysis provided a guidance as for how wide the DSD saw-cut was needed near the center frame of the panel, so that the edges of the DSD did not come in contact before the final failure occurred. It correctly identified the locations of the first damage initiation at the tips of the saw-cut and also the critical locations near the flanges of the side frames (rather than at the frame tops) in the vicinity of the DSD. The analysis also correctly predicted that the side frames and the T-caps of the crown panel would not buckle, but would fail by crushing (i.e., fail by exceeding strength capabilities rather than in the stability mode). The above information was used to make informed choices with regard to locations of additional strain gauges near the DSD and also with regard to the extent of the crown panel area for which the full-field VIC-3D measurements would be acquired.

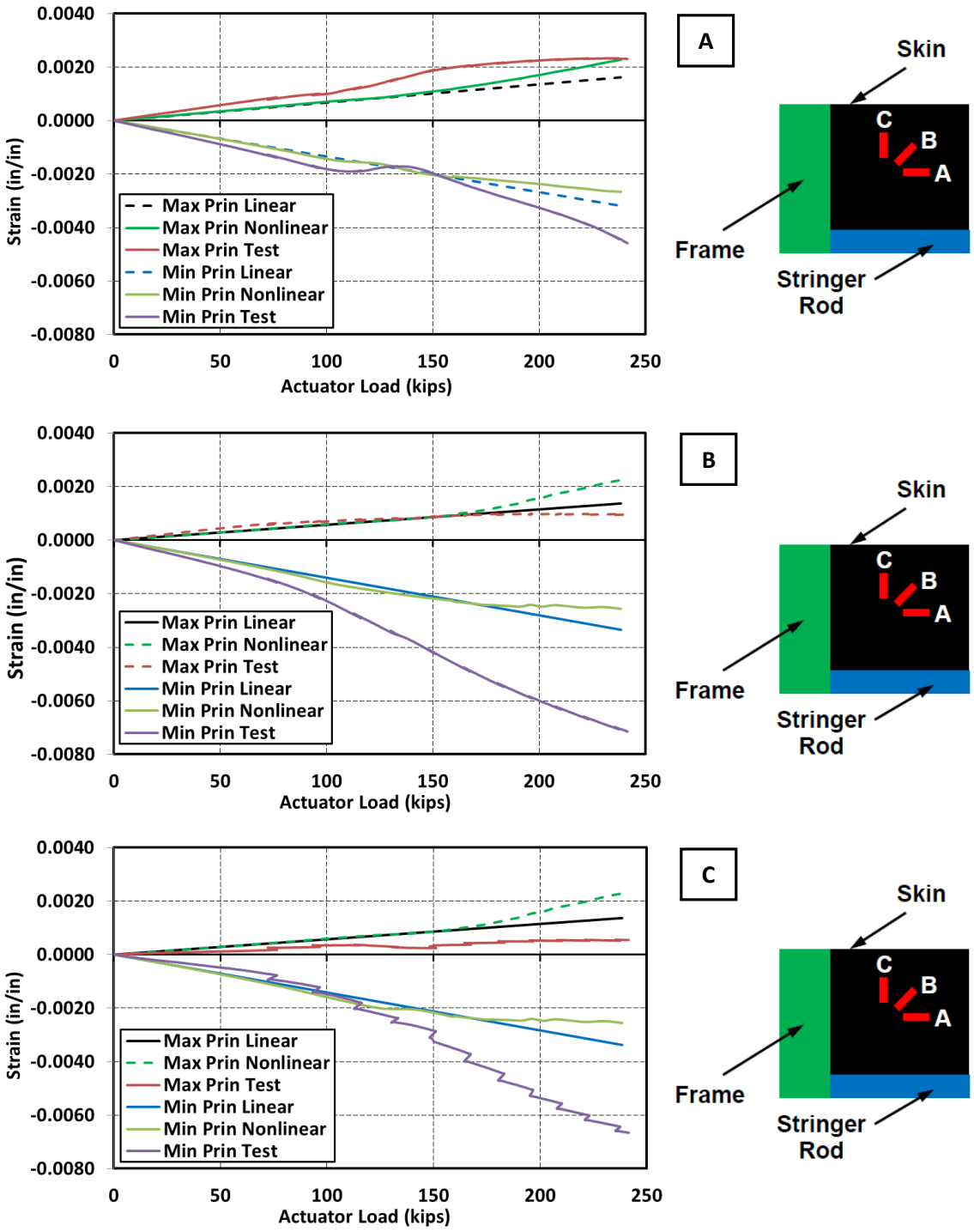

Figure 27. Principal strains in the upper bulkhead panel skin (top: sg05108A/sg05109B/sg05110C, middle: sg05111A/sg05112B/sg05113C, and bottom: sg05117A/sg05118B/sg05119C).

Acknowledgments

The authors acknowledge the entire team from The Boeing Company who built the test article and worked with the NASA Langley Research Center personnel in support of the testing activities. Contributions of Alex Velicki, Kim Linton, Krishna Hoffman, Patrick Thrash, Jaime Baraja, and Andy Harber from Boeing Research and Technology, Huntington Beach, California are particularly acknowledged. Support of the testing effort by David Dawicke and Nathaniel Gardner (Analytical Services and Materials, Inc.) and Michael McNeil (Science and Technology Corporation) is also gratefully acknowledged.

References

[1]Li, V. and Velicki, A., "Advanced PRSEUS Structural Concept Design and Optimization," *Proceedings of the 12th AIAA/ISSMO Multidisciplinary Analysis and Optimization Conference*, AIAA-2008-5840, Victoria, BC, Canada, September 2008.

[2]Jegley, D. C., Velicki, A., and Hansen, D. A., "Structural Efficiency of Stitched Rod-Stiffened Composite Panels with Stiffener Crippling," *Proceedings of the 49th AIAA/ASME/ASCE/AHS/ASC Structures, Structural Dynamics and Materials Conference*, AIAA-2008-2170, Schaumburg, IL, April 2008.

[3]Velicki, A., Thrash, P. J., and Jegley, D. C., "Airframe Development for the Hybrid Wing Body Aircraft," *Proceedings of the 47th AIAA Aerospace Sciences Meeting Including The New Horizons Forum and Aerospace Exposition*, AIAA-2009-932, Orlando, FL, January 2009.

[4]Yovanof, N. P., Velicki A. and Li, V., "Advanced Structural Stability Analysis of a Nonlinear BWB-Shaped Vehicle," *Proceedings of the 50th AIAA/ASME/ASCE/AHS/ASC Structures, Structural Dynamics and Materials Conference*, AIAA-2009-2452, Palm Springs, CA, May 2009.

[5]Velicki, A. and Thrash, P. J., "Advanced Structural Concept Development Using Stitched Composites," *Proceedings of the 49th AIAA/ASME/ASCE/AHS/ASC Structures, Structural Dynamics and Materials Conference*, AIAA-2008-2329, Schaumburg, IL, April 2008.

[6]Thrash, P. J., "Manufacturing of a Stitched Resin Infused Fuselage Test Article," *Proceedings of the Composites and Advanced Materials Expo*, Orlando, FL, October 2014.

[7]Velicki, A., "Damage Arresting Composites for Shaped Vehicles, Phase I Final Report," NASA CR-2009-215932, NASA Langley Research Center, Hampton, VA, 2009.

[8]Lovejoy, A. E., Rouse, M., Linton, K. A., and Li, V.P., "Pressure Testing of a Minimum Gauge PRSEUS Panel," *Proceedings of the 52nd AIAA/ASME/ASCE/AHS/ASC Structures, Structural Dynamics and Materials Conference*, AIAA-2011-1813, Denver, CO, April 2011.

[9]Velicki, A., Yovanof, N. P., Baraja, J., Linton, K. A., Li, V., Hawley, A., Thrash, P., DeCoux, S., and Pickell, R., "Damage Arresting Composites for Shaped Vehicles – Phase II Final Report," NASA CR-2011-216880, NASA Langley Research Center, Hampton, VA, 2011.

[10]Velicki, A. and Jegley, D. C., "PRSEUS Development for the Hybrid Wing Body Aircraft," *Proceedings of the AIAA Centennial of Naval Aviation Forum "100 Years of Achievement and Progress,"* AIAA-2011-7025, Virginia Beach, VA, September 2011.

[11]Yovanof, N., Baraja, J, Lovejoy, A. E., and Gould, K. E., "Design, Analysis, and Testing of a PRSEUS Pressure Cube to Investigate Assembly Joints," *Proceedings of the 2012 Aircraft Airworthiness and Sustainment Conference*, TP5431, Baltimore, MD, April 2012.

[12]Yovanof, N. and Jegley, D. C., "Compressive Behavior of Frame-Stiffened Composite Panels," *52nd AIAA/ ASME/ASCE/AHS/ASC Structures Dynamics and Materials Conference*, AIAA-2011-1913, Denver, CO, April 2011.

[13]Przekop, A. and Jegley, D. C., "Testing and Analysis Validation of a Metallic Repair Applied to a PRSEUS Tension Panel," *Proceedings of the 54th AIAA/ASME/ASCE/AHS/ASC Structures, Structural Dynamics and Materials Conference*, AIAA-2013-1735, Boston, MA, April 2013.

[14]Jegley, D. C. and Velicki, A., "Status of Advanced Stitched Unitized Composite Aircraft Structure," *Proceedings of the 51st AIAA Aerospace Sciences Meeting*, AIAA 2013-0410, Grapevine, TX, January 2013.

[15]Velicki, A. and Thrash, P. J., "Damage Arrest Design Approach Using Stitched Composites," *The Aeronautical Journal*, Vol. 115, No. 1174, pp. 789-795, Royal Aeronautical Society, London, UK, December 2011.

[16]Bergan, A., Bakuckas, J., Lovejoy, A. E, Jegley, D. C., Linton, K. A., Korkosz, G., Awerbuch, J., and Tan, T., "Full-Scale Test and Analysis of a PRSEUS Fuselage Panel to Assess Damage-Containment Features," *Proceedings of the 2011 Aircraft Airworthiness and Sustainment Conference*, TP4558, San Diego, CA, April 2011.

[17]Velicki, A. and Thrash P. J., "Blended Wing Body Structural Concept Development," *Proceedings of Aircraft Structural Design Conference*, Liverpool, UK, October 2008.

[18]Przekop, A., Jegley, D. C., Lovejoy, A. E., Rouse, M., and Wu, H. Y., "Testing and Analysis of a Composite Non-Cylindrical Aircraft Fuselage Structure, Part I: Ultimate Design Loads," *Proceedings of the 57th AIAA/ASME/ASCE/ AHS/ASC Structures, Structural Dynamics and Materials Conference*, AIAA-2016-2176, San Diego, CA, January 2016.

[19]Ambur, D. A., Rouse, M., Starnes, J. H., and Stuart, M. J., "Facilities for Combined Loads Testing of Aircraft Structures to Satisfy Structural Technology Development Requirements," *Proceedings of the 5th Annual Advanced Composites Technology Conference*, Seattle, WA, August 1994.

[20]Przekop, A., Jegley, D. C., Rouse, M., and Lovejoy, A. E., "Finite Element Analysis and Test Results Comparison for the Hybrid Wing Body Center Section test Article," NASA TM-2016-218973, NASA Langley Research Center, Hampton, VA, 2016.

[21]Wu, H. T., Shaw, P., and Przekop, A., "Analysis of a Hybrid Wing Body Center Section Test Article," *Proceedings of the 54th AIAA/ASME/ASCE/AHS/ASC Structures, Structural Dynamics and Materials Conference*, AIAA-2013-1734, Boston, MA, April 2013.

[22]Przekop, A., Wu, H. T., and Shaw, P., "Nonlinear Finite Element Analysis of a Composite Non-Cylindrical Pressurized Aircraft Fuselage Structure," *Proceedings of the 55th AIAA/ASME/ASCE/AHS/ASC Structures, Structural Dynamics and Materials Conference*, AIAA-2014-1064, National Harbor, MD, January 2014.

[23]MSC Nastran 2012.2 Quick Reference Guide, MSC Software Corporation, Santa Ana, CA, 2012.

[24]Title 14 Code of Federal Regulation, Part 25 "Airworthiness Standards: Transport Category Airplanes," Subpart C "Structure," Electronic Code of Federal Regulations, http://www.ecfr.gov/cgi-bin/text-idx?c=ecfr&tpl =/ecfrbrowse/Title14/14cfr25_main_02.tpl

[25]McGowan, D. M., Ambur, D. R., and McNeil, S. R., "Full-field Structural Response of Composite Structures: Analysis and Experiment," *Proceedings of the 44th AIAA/ASME/ASCE/AHS/ASC Structures, Structural Dynamics and Materials Conference*, AIAA 2003-1623, Norfolk, VA, April 2003.

[26]Moore, J. P., Przekop, A., Juarez, P. D., and Roth, M. C., "Fiber Optic Rosette Strain Gauge Development and Application on a Large-Scale Composite Structure," NASA TM-2016-218970, NASA Langley Research Center, Hampton, VA, 2016.

[27]Horne, M. R. and Madaras, E., "Evaluation of Acoustic Emission SHM of PRSEUS Multi-Bay Box Tests," NASA TM-2016-218976, NASA Langley Research Center, Hampton, VA, 2016.

[28]Johnston, P. H. and Juarez, P. D., "Nondestructive Evaluation of PRSEUS During Large-Scale Load Testing and Rod Push-Out Testing," NASA TM-2016-218978, NASA Langley Research Center, Hampton, VA, 2016.

[29]Jegley, D. C., Przekop, A., Rouse, M., Lovejoy, A. E., Velicki, A., Linton, K., Wu, H. T., Baraja, J., Thrash, P., and Hoffman, K., "Development of Stitched Composite Structure for Advanced Aircraft," *Proceedings of the American Society for Composites 30th Technical Conference*, Paper 1840, East Lansing, MI, September 2015.

[30]Jegley, D. C., Rouse, M., Przekop, A., and Lovejoy, A. E., "The Behavior of a Stitched Composite Large-Scale Multi-Bay Pressure Box," NASA TM-2016-218972, NASA Langley Research Center, Hampton, VA, 2016.